5 The Solar System

R. Lynne Jones, Steven R. Chesley, Paul A. Abell, Michael E. Brown, Josef Ďurech, Yanga R. Fernández, Alan W. Harris, Matt J. Holman, Željko Ivezić, R. Jedicke, Mikko Kaasalainen, Nathan A. Kaib, Zoran Knežević, Andrea Milani, Alex Parker, Stephen T. Ridgway, David E. Trilling, Bojan Vršnak

LSST will provide huge advances in our knowledge of millions of astronomical objects "close to home"– the small bodies in our Solar System. Previous studies of these small bodies have led to dramatic changes in our understanding of the process of planet formation and evolution, and the relationship between our Solar System and other systems. Beyond providing asteroid targets for space missions or igniting popular interest in observing a new comet or learning about a new distant icy dwarf planet, these small bodies also serve as large populations of "test particles," recording the dynamical history of the giant planets, revealing the nature of the Solar System impactor population over time, and illustrating the size distributions of planetesimals, which were the building blocks of planets.

In this chapter, a brief introduction to the different populations of small bodies in the Solar System (§ 5.1) is followed by a summary of the number of objects of each population that LSST is expected to find (§ 5.2). Some of the Solar System science that LSST will address is presented through the rest of the chapter, starting with the insights into planetary formation and evolution gained through the small body population orbital distributions (§ 5.3). The effects of collisional evolution in the Main Belt and Kuiper Belt are discussed in the next two sections, along with the implications for the determination of the size distribution in the Main Belt (§ 5.4) and possibilities for identifying wide binaries and understanding the environment in the early outer Solar System in § 5.5. Utilizing a "shift and stack" method for delving deeper into the faint end of the luminosity function (and thus to the smallest sizes) is discussed in § 5.6, and the likelihood of deriving physical properties of individual objects from light curves is discussed in the next section (§ 5.7). The newly evolving understanding of the overlaps between different populations (such as the relationships between Centaurs and Oort Cloud objects) and LSST's potential contribution is discussed in the next section (§ 5.8). Investigations into the properties of comets are described in § 5.9, and using them to map the solar wind is discussed in § 5.10. The impact hazard from Near-Earth Asteroids (§ 5.11) and potential of spacecraft missions to LSST-discovered Near-Earth Asteroids (§ 5.12) concludes the chapter.

5.1 A Brief Overview of Solar System Small Body Populations

Steven R. Chesley, Alan W. Harris, R. Lynne Jones

A quick overview of the different populations of small objects of our Solar System, which are generally divided on the basis of their current dynamics, is:

- **Near-Earth Asteroids (NEAs)** are defined as any asteroid in an orbit that comes within 1.3 astronomical unit (AU) of the Sun (well inside the orbit of Mars). Within this group, a subset in orbits that pass within 0.05 AU of the Earth's orbit are termed **Potentially Hazardous Asteroids (PHAs)**. Objects in more distant orbits pose no hazard of Earth impact over the next century or so, thus it suffices for impact monitoring to pay special attention to this subset of all NEAs. Most NEAs have evolved into planet-crossing orbits from the Main Asteroid Belt, although some are believed to be extinct comets and some are still active comets.
- Most of the inner Solar System small bodies are **Main Belt Asteroids (MBAs)**, lying between the orbits of Mars and Jupiter. Much of the orbital space in this range is stable for billions of years. Thus objects larger than 200 km found there are probably primordial, left over from the formation of the Solar System. However, the zone is crossed by a number of resonances with the major planets, which can destabilize an orbit in that zone. The major resonances are clearly seen in the distribution of orbital semi-major axes in the Asteroid Belt: the resonances lead to clearing out of asteroids in such zones, called Kirkwood gaps. As the Main Belt contains most of the stable orbital space in the inner Solar System and the visual brightness of objects falls as a function of distance to the fourth power (due to reflected sunlight), the MBAs also compose the majority of observed small moving objects in the Solar System.
- **Trojans** are asteroids in 1:1 mean-motion resonance with any planet. Jupiter has the largest group of Trojans, thus "Trojan" with no clarification generally means Jovian Trojan ("TR5" is also used below as an abbreviation for these). Jovian Trojan asteroids are found in two swarms around the L4 and L5 Lagrangian points of Jupiter's orbit, librating around these resonance points with periods on the order of a hundred years. Their orbital eccentricity is typically smaller (<0.2) than those of Main Belt asteroids, but the inclinations are comparable, with a few known Trojans having inclinations larger than 30 degrees. It seems likely that each planet captured planetesimals into its Trojan resonance regions, although it is not clear at what point in the history of the Solar System this occurred or how long objects remain in Trojan orbits, as not all Trojan orbits are stable over the lifetime of the Solar System.
- Beyond Neptune, the **Trans-Neptunian Objects (TNOs)** occupy a large area of stable orbital space. When these objects were first discovered, it was thought that they were truly primordial remnants of the solar nebula, both dynamically and chemically primordial. Further discoveries proved that this was not the case and that the TNOs have undergone significant dynamical processing over the age of the Solar System. Recent models also indicate that they are likely to have been formed much closer to the Sun than their current location, as well as being in high relative velocity, collisionally erosive orbits. Thus, they are likely to also have undergone chemical processing. TNOs can be further broken down into **Scattered Disk Objects (SDOs)**, in orbits which are gravitationally interacting with Neptune (typically $e > 0.3$, $q < 38$ AU); **Detached Objects**, with perihelia beyond the gravitational perturbations of the giant planets; **Resonant Objects**, in mean-motion resonance (MMR) with Neptune (notably the "Plutinos," which orbit in the 3:2 MMR like Pluto); and the **Classical Kuiper Belt Objects (cKBOs)**, which consist of the objects with $32 < a < 48$ AU on stable

orbits not strongly interacting with Neptune (see Gladman et al. 2008 for more details on classification within TNO populations). The **Centaurs** are dynamically similar in many ways to the SDOs, but the Centaurs cross the orbit of Neptune.

- **Jupiter-family comets (JFCs)** are inner Solar System comets whose orbits are dominantly perturbed by Jupiter. They are presumed to have derived from the Kuiper Belt in much the same manner as the Centaur population. These objects are perturbed by the giant planets into orbits penetrating the inner Solar System and even evolve into Earth-crossing orbits. The Centaurs may be a key step in the transition from TNO to JFC. The JFCs tend to have orbital inclinations that are generally nearly ecliptic in nature. A second class of comets, so-called **Long Period comets (LPCs)**, come from the **Oort Cloud (OC)** 10,000 or more AU distant, where they have been in "deep freeze" since the early formation of the planetary system. Related to this population are the **Halley Family comets (HFCs)**, which may also originate from the Oort Cloud, but have shorter orbital periods (traditionally under 200 years). Evidence suggests that some of these HFCs may be connected to the **Damocloids**, a group of asteroids that have dynamical similarities to the HFCs, and may be inactive or extinct comets. A more or less constant flux of objects in the Oort Cloud is perturbed into the inner Solar System by the Galactic tide, passing stars, or other nearby massive bodies to become the LPCs and eventually HFCs. These comets are distinct from JFCs by having very nearly parabolic orbits and a nearly isotropic distribution of inclinations. Somewhat confusingly, HFCs and JFCs are both considered "short-period comets" (SPCs) despite the fact that they likely have different source regions.

5.2 Expected Counts for Solar System Populations

Željko Ivezić, Steven R. Chesley, R. Lynne Jones

In order to estimate expected LSST counts for populations of small solar system bodies, three sets of quantities are required:

1. the LSST sky coverage and flux sensitivity;
2. the distribution of orbital elements for each population; and
3. the absolute magnitude (size) distribution for each population.

Discovery rates as a function of absolute magnitude can be computed from a known cadence and system sensitivity without knowing the actual size distribution (the relevant parameter is the difference between the limiting magnitude and absolute magnitude). For an assumed value of absolute magnitude, or a grid of magnitudes, the detection efficiency is evaluated for each modeled population. We consider only observing nights when an object was observed at least twice, and consider an object detected if there are three such pairs of detections during a single lunation. The same criterion was used in recent NASA NEA studies.

Figure 5.1 summarizes our results, and Table 5.2 provides differential completeness (10%, 50%, 90%) values at various H magnitudes[1]. The results essentially reflect the geocentric (and for

[1]The absolute magnitude H of an asteroid is the apparent magnitude it would have 1 AU from both the Sun and the Earth with a phase angle of 0°.

NEAs, heliocentric), distance distribution of a given population. The details in orbital element distribution are not very important, as indicated by similar completeness curves for NEAs and PHAs, and for classical and scattered disk TNOs.

The next subsections provide detailed descriptions of the adopted quantities.

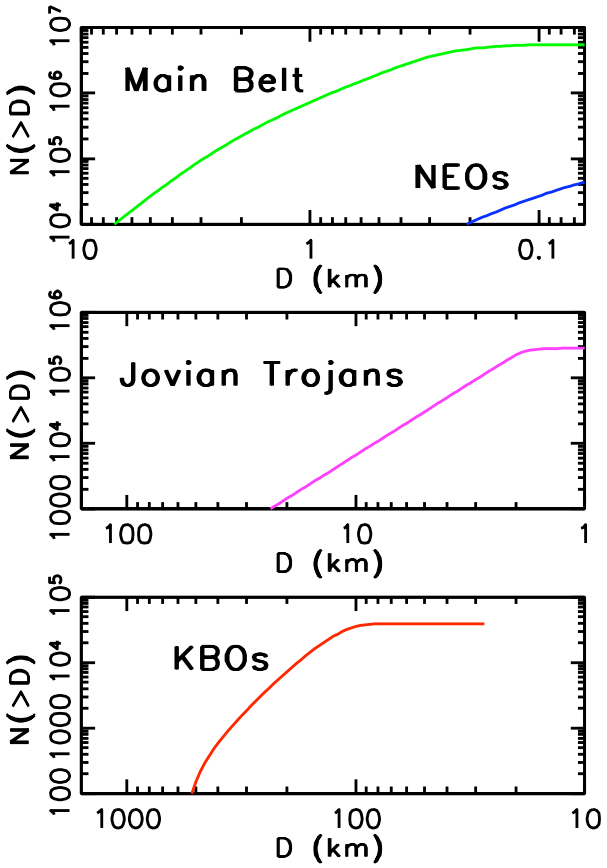

Figure 5.1: Cumulative counts of asteroids detected by LSST vs. size for dominant populations of Solar System bodies, as marked. The total expected numbers of objects detected by LSST are 5.5 million Main Belt asteroids, 100,000 NEAs, 280,000 Jovian Trojans, and 40,000 TNOs (marked KBO).

5.2.1 LSST Sky Coverage and Flux Sensitivity

A detailed discussion of the LSST flux limits for moving objects and impact of trailing losses is presented in Ivezić et al. (2008), §3.2.2. Here we follow an identical procedure, except that we extend it to other Solar System populations: Near-Earth Asteroids, Main Belt asteroids, Jovian Trojans, and TNOs.

The sky coverage considered for the cumulative number of objects in each population includes the universal cadence fields and the northern ecliptic spur, as well as the "best" pairs of exposures from the deep drilling fields. However, the increased depth in the deep drilling fields which is possible

Table 5.1: Absolute magnitude at which a given detection completeness is reached[a]

Population	H(90%)	H(50%)	H(10%)	N^b_{LSST}
PHA	18.8	22.7	25.6	—
NEA	18.9	22.4	24.9	100,000
MBA	20.0	20.7	21.9	5.5 million
TR5	17.5	17.8	18.1	280,000
TNO	7.5	8.6	9.2	40,000
SDO	6.8	8.3	9.1	—

[a]Table lists absolute magnitude H values at which a differential completeness of 90%, 50% or 10% is reached. This is not a cumulative detection efficiency (i.e. completeness for $H > X$), but a differential efficiency (i.e. completeness at $H = X$). [b]Approximate total number of objects detected with LSST, in various populations. PHAs and SDOs are included in the counts of NEAs and TNOs.

from co-adding the exposures using shift-and-stack methods is not considered here. Instead, the results of deep drilling are examined in § 5.6.

5.2.2 Assumed Orbital Elements Distributions

We utilize orbital elements distributed with the MOPS code described in § 2.5.3. The MOPS code incorporates state-of-the-art knowledge about various Solar System populations (Grav et al. 2009). The availability of MOPS synthetic orbital elements made this analysis fairly straightforward. In order to estimate the efficiency of LSST cadence for discovering various populations, we extract 1000 sets of orbital elements from MOPS for each of the model populations of NEAs, PHAs, MBAs, Jovian Trojans, TNOs and SDOs.

Using these orbital elements, we compute the positions of all objects at the time of all LSST observations listed in the default cadence simulation (see § 3.1). We use the JPL ephemeris code implemented as described in Jurić et al. (2002). We positionally match the two lists and retain all instances when a synthetic object was within the field of view. Whether an object was actually detected or not depends on its assumed absolute magnitude, drawn from the adopted absolute magnitude distribution (see § 5.2.3).

These orbital element distributions are, of course, only approximate. However, they represent the best current estimates of these populations, and are originated from a mixture of observations and theoretical modeling. This technique provides an estimate of the fraction of detectable objects in each population, at each absolute magnitude. The results of this analysis are shown in Figure 5.2.

5.2.3 The Absolute Magnitude Distributions

LSST's flux limit will be about five magnitudes fainter that the current completeness of various Solar System catalogs. Hence, to estimate expected counts requires substantial extrapolation of

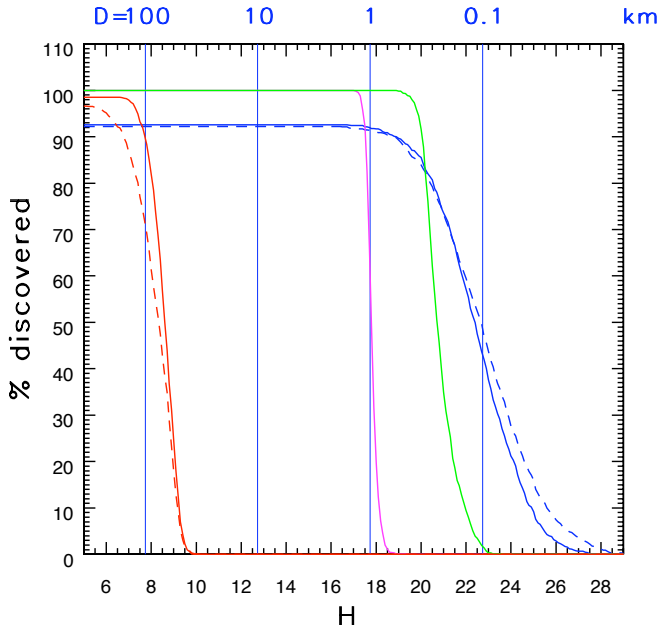

Figure 5.2: A comparison of LSST discovery efficiency for dominant populations of Solar System bodies. Solid lines correspond to classical TNOs (red), Jovian Trojans (magenta), Main Belt Asteroids (green), and NEAs (blue). The red dashed line corresponds to scattered disk objects, and the blue dashed line to PHAs. Note that the completeness for NEAs and PHAs does not reach 100% even for exceedingly large objects (due to finite survey lifetime).

known absolute magnitude distributions. We adopt the following cumulative distributions, which are illustrated in Figure 5.3.

For MBAs, we adopt the shape of the cumulative counts curve based on SDSS data and given by Equation 12 of Ivezić et al. (2001), including their normalization of 774,000 objects larger than $D = 1$ km

$$N_{cum}^{MBA} = 267,000 \frac{10^{0.43x}}{10^{0.18x} + 10^{-0.18x}}, \tag{5.1}$$

where $x = H - 15.7$ and a fiducial albedo of 0.14 is assumed (so that $H = 22$ corresponds to a size of 140 m, as discussed in the NEA context, see § 5.11). This normalization agrees within 10% with the (Durda & Dermott 1997) result that there are 67,000 objects with $H < 15.5$ (assuming a mean albedo for MBAs of 0.10), and is consistent at the same level with the latest SDSS results (Parker et al. 2008). This approach is accurate to only several tens of a percent, because the shape of the count vs. H curve varies across the belt and between families and background, as well as among individual families. At this level of accuracy, there are about a million Main Belt Asteroids larger than 1 km. We note that the MOPS normalization implies twice as many objects as given by this normalization. About half of this discrepancy could be due to faulty H values in contemporary asteroid catalogs (for more details, see Parker et al. 2008). For other populations, we adopt the cumulative counts implemented in MOPS.

For NEAs, we adopt the Bottke et al. (2002) result

$$N_{cum}^{NEA} = 960 \times 10^{0.35(H-18)}. \tag{5.2}$$

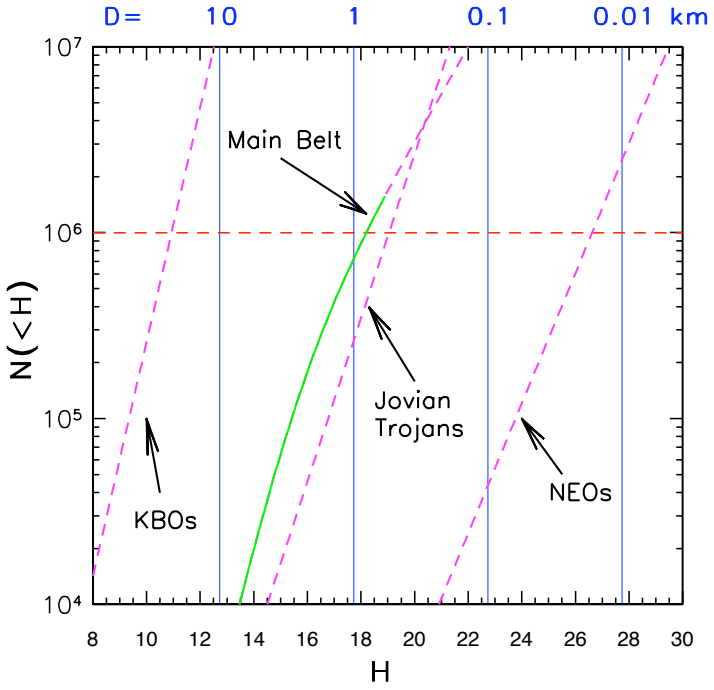

Figure 5.3: A comparison of cumulative count vs. absolute magnitude curves for dominant populations of Solar System bodies. The solid portion of the line for Main Belt Asteroids signifies directly constrained counts; all dashed lines are extrapolations from brighter H. The horizontal line at $N = 10^6$ is added to guide the eye. The object diameters marked on top correspond to an albedo of 0.14. Populations with low median albedo, such as Jovian Trojans and TNOs, have 2-3 times larger D for a given H. In particular, there are comparable numbers of Main Belt Asteroids and Jovian Trojans down to the same *size* limit.

For Jovian Trojans, we adopt the Szabó et al. (2007) result

$$N_{cum}^{Tr5} = 794 \times 10^{0.44(H-12)}. \tag{5.3}$$

This expression was constrained using SDSS data to $H = 14$, and implies similar counts of Jovian Trojans and Main Belt Asteroids down to the same size limit, for sizes larger than ∼10 km. Note that this does not imply similar observed number counts of Jovian Trojans and MBAs, since the Main Belt is much closer. The extrapolation of this expression to $H > 14$ may be unreliable. In particular, the Jovian Trojan counts become much larger than the cumulative counts of MBAs for $H > 20$, because the counts slope at the faint end becomes smaller for the latter. A recent study based on SDSS data by Szabó & Kiss (2008) demonstrated that existing moving object catalogs are complete to $r \sim 19.5$, or to a size limit of about 20 km, giving a total count of the order a thousand known Jovian Trojans.

For TNOs, we adopt results obtained by Trujillo et al. (2000, 2001)

$$N_{cum}^{TNO} = 71,400 \times 10^{0.63(H-9.1)}, \tag{5.4}$$

where we assumed a normalization of 71,400 objects larger than 100 km, and an albedo of 0.04. This normalization includes classical, scattered disk and resonant TNOs, with equal numbers of classical and resonant objects and 0.8 Scattered Disk Objects per classical TNO.

5.2.4 Expected Cumulative Counts

Given the adopted cumulative counts (§ 5.2.3) and completeness curves (§ 5.2.2), it is straightforward to generate the expected observed counts. Table 5.2 provides the expected LSST sample size for each population.

Unsurprisingly, the largest observed sample will be MBAs, which will be probed to a size limit as small as ~ 100 m. It is remarkable that the Jovian Trojan sample will include $\sim 280,000$ objects, on the order of the number of currently known MBAs – currently there are only a few thousand known Jovian Trojans. In addition, the expected detection of 40,000 objects in the TNO sample, with accurate color and variability measurements for a substantial fraction of these objects, will enable investigation of these distant worlds with a thoroughness that is currently only possible for MBAs.

Figure 5.4 shows the median number of expected LSST observations (based on the Operations Simulator; § 3.1) for dominant populations of Solar System bodies. We do not include nights with only one detection. A significant fraction of discovered objects will have several hundred detections. For example, more than 150 observations will be available for about 500 NEAs, one million MBAs, 50,000 Jovian Trojans and 7,000 TNOs. The corresponding counts for objects with more than 100 observations are 1,400 NEAs, 1.6 million MBAs, 80,000 Jovian Trojans, and 11,000 TNOs. These large numbers of multi-color light curves will enable numerous novel research directions in studies such as light-curve inversion for a significant fraction of these Solar System populations.

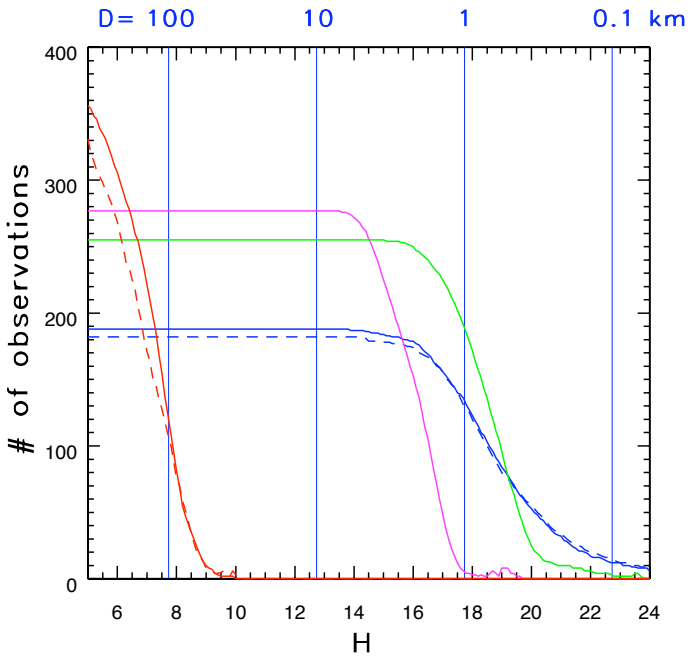

Figure 5.4: The median number of expected LSST detections of a given object as a function of H for dominant populations of Solar System bodies. Solid lines correspond to classical TNOs (red), Jovian Trojans (magenta), MBAs (green), and NEAs (blue). The red dashed line corresponds to Scattered Disk Objects, and the blue dashed line to PHAs. Nights with only one detection are not counted.

5.3 The Orbital Distributions of Small Body Populations

R. Lynne Jones, Michael E. Brown

LSST will produce large catalogs of well-measured orbits for moving objects throughout the Solar System from NEAs to TNOs. These orbital catalogs are important for many reasons, the most obvious of which is the necessity of predicting highly accurate ephemerides (positions and magnitudes) for the study of individual objects in greater detail. Just as (or more) important, however, is the study of the ensemble of orbits (as the distribution of orbital parameters) in order to understand the current state and previous evolution of each population of small bodies, as this is inextricably linked to the evolution of the giant planets. Information about this evolution is preserved in the orbital parameters of the small bodies.

The importance of this record was first clearly realized when the discovery of large numbers of TNOs in mean-motion resonance with Neptune, together with the discovery of giant extrasolar planets at small distances from their stars, created a new vision of our Solar System. Instead of a static place, where the giant planets formed in their current locations, Malhotra (1995) proposed that a gradual outward migration in Neptune's orbit could have gathered TNOs into 2:3 mean-motion resonance (MMR) with Neptune. This migration trapped TNOs (Plutinos in this resonance) into the 2:3 MMR resonance at a density higher than in the rest of the Kuiper Belt. In this new vision of a more dynamic Solar System, the orbital distributions of large populations of small bodies serve as "test particles" and preserve an invaluable fossil record of the orbital evolution of the giant planets.

In recent years, the Nice model (Tsiganis et al. 2005) has proposed that all giant planets formed at less than 14 AU from the Sun and the solar nebula was truncated near 30 AU. The giant planets and small bodies in the Solar System subsequently evolved to their current state through planetary migration due to angular momentum exchange with planetesimals. The Nice model presents an intriguing theory which could account for many previously unexplained problems in various small body populations: the mass depletion observed in the Kuiper Belt (Levison et al. 2008b) and the Asteroid Belt (O'Brien et al. 2007), the orbital distribution of Trojans (Morbidelli et al. 2005), and the late heavy bombardment (Gomes et al. 2005). However, the Nice model has no obvious way to produce the detached TNOs with perihelion beyond 50 AU (such as 2004 XR_{190}) and also has problems reproducing the orbital distribution (particularly the inclinations) of the cold classical Kuiper Belt.

There are other older but still competitive theories: models related to the slow planetary migration first detected in the Plutino fraction (Gomes 2003; Gomes et al. 2004; Hahn & Malhotra 2005), models where a rogue planetary embryo or large planetesimal pass through or orbit briefly in the outer Solar System (Petit et al. 1999; Gladman & Chan 2006), or models of nearby stellar passages early in the history of the Solar System (Ida et al. 2000; Kenyon & Bromley 2004; Morbidelli & Levison 2004; Brasser et al. 2008; Kaib & Quinn 2008). Each of these theories has particular strengths. The stellar flyby model is able to produce objects with large semi-major axes, high perihelions, and high eccentricities such as Sedna. The rogue planetary embryo model is able to produce objects like 2004 XR_{190} with perihelion beyond the reach of Neptune's perturbation, high inclination or eccentricity, but semi-major axis just outside the classical belt, without perturbing the classical belt as strongly as the stellar flyby model would. The slow migration model can drop

objects into low eccentricity orbits, perhaps even to the level of creating the dynamically cold classical belt, while creating a distribution of inclinations. A major problem with all of these theories beyond various problems recreating specifics of the inclination and eccentricity distributions is that the mass required to build the largest objects we see in the Kuiper Belt today is much larger than the total mass detected (Stern & Colwell 1997); therefore the mass must have been depleted somehow. The amount of mass depletion required would likely have left its trace in the orbit of Neptune (Gomes et al. 2004), resulting in a different orbit than observed today (circular at 30 AU). However, none of these models has been conclusively ruled out, and it seems likely that one or more of these mechanisms has contributed to the current distribution of TNOs, in particular since migration is known to have occurred in some form, and passing stars in the solar birth environment is likely (Lada & Lada 2003).

It becomes clear from this range of models that can potentially fit the available data that the current statistical sample of TNOs ($< 2,000$ objects) is unable to make strong distinctions among the theories. With a vastly increased sample size, LSST will provide much stronger statistical tests. In particular, the inclination and eccentricity distributions of the classical belt will be well measured, along with obtaining *griz* color measurements for further understanding of the "cold" and "hot" classical belt members – this alone should provide strong constraints on the Nice model and determine whether a rogue embryo or planetesimal must have passed through the primordial Kuiper Belt. By measuring the perihelion distribution of Scattered Disk Objects to greater distances (LSST can detect objects down to 400 km in diameter as far as 100 AU assuming an albedo of 0.1) and larger amounts of sky than currently possible, LSST will provide direct tests of the stellar flyby models.

In addition, the detection of "rare" objects can provide strong leverage to distinguish among models, or even rule out theories which are unable to create such objects. As an example of a currently known rare population, there are a handful of TNOs, called "detached" TNOs (Gladman et al. 2008), which generally show the signature of some strong dynamical perturbation in the past through a current high eccentricity or inclination but without a strong indication of the cause of this perturbation. As the detached TNOs have perihelia beyond ~ 45 AU, the perturbations cannot be due to gravitational interaction with the giant planets. For some of these detached objects, such as 2000 CR_{105} (Gladman et al. 2002) or Sedna (Brown et al. 2004) (whose orbit is entirely contained beyond the outer edge of the classical Kuiper Belt, ~ 50 AU, and inside the inner edge of the Oort Cloud, $\sim 20,000$ AU), interaction with a passing star seems the most likely cause (Morbidelli & Levison 2004). For others, such as 2004 XR_{190} (Allen et al. 2006) or 2008 KV_{42} (Gladman et al. 2009) (the first known retrograde TNO, having an inclination of 102°), the source of the perturbation is much less clear. A complication in the interpretation of these unusual objects is knowing if the newly discovered TNO is just an unlikely outlier of an underlying distribution, or if it truly is the "first discovery of its kind." Many of these problems in interpretation are due to observational selection biases in flux, inclination, and observational followup (Kavelaars et al. 2008) or miscalculated orbits (Jones et al. 2009). For example, retrograde TNOs are not only difficult to detect due to their apparent rarity, but in a short series of observations (a few days), the orbit can appear to be that of a much more common nearby high-eccentricity asteroid instead of a distant retrograde or high-inclination TNO. The frequent observing schedule and well-characterized in limiting magnitude and sky coverage of LSST will minimize the effect of these biases. With the total sample size of $\sim 40,000$ TNOs expected by LSST, it will also be possible to characterize these rare objects, which likely compose at most a few percent of the observed population.

In general, a large sample of TNOs with well-measured orbits, detected in a well-characterized survey, will provide strong statistical tests for the current theories of Solar System evolution and strong pointers to where the models need to go for the next generation of theories.

These tests can be carried on into the inner Solar System, although in these regions the populations have been much more strongly affected by perturbations from the planets. For example, resonances in the Main Asteroid Belt were long ago cleared of primordial objects, since these resonances are unstable to gravitational perturbations from Jupiter. Asteroids which chance to drift into these zones (i.e., by Yarkovsky drift), will be promptly removed by resonant perturbations to become planet-crossing, and from there suffer collision or ejection by close encounters with major planets. Interestingly, the Main Belt itself seems to have been severely depleted of mass, beyond the expected losses due to ejection by gravitational perturbation from the planets in their current locations. The Main Belt inclination distribution also has been dynamically excited, in a manner similar to the classical Kuiper Belt. Theories to explain this mass depletion and/or dynamical excitation include similar models as used to explain the mass depletion or dynamical excitation of the Kuiper Belt – a planetary embryo (or large planetesimal) passing through the region (Petit et al. 2001), secular resonances sweeping through the Main Belt (Nagasawa et al. 2000), or gravitational perturbations resulting from the large-scale rearrangement of the Solar System occurring during the rapid evolution phase of the Nice model (O'Brien et al. 2007; Minton & Malhotra 2009). In the Asteroid Belt, the colors of objects are strongly correlated with the history of the object's formation and dynamical evolution, suggesting that obtaining *griz* colors as well as orbital parameters will provide further strong constraints for these models.

The orbital distribution of Jovian Trojans also provides useful constraints on the environment of the early Solar System. One hypothesis for the origin of the Trojans is that they were formed simultaneously with Jupiter and then captured and stabilized near the growing Jupiter's L4 and L5 points (Peale 1993). An alternative hypothesis suggests they were captured over a much longer period after forming elsewhere in the Solar System (Jewitt 1996). The colors of many known Trojans are similar to SDOs from the outer Solar System and others appear similar to the colors of outer MBAs, as in Figure 5.5, lending support to the second hypothesis, with implications for the importance of gas drag in the early Solar System. The Nice model suggests a more complex picture, where the present permanent Trojan population is built up by planetesimals trapped after the 1:2 mean-motion resonance crossing of Saturn and Jupiter (Morbidelli et al. 2005).

A clear picture of the orbital distribution of small bodies throughout the entire Solar System would provide the means to test each of these models and provide constraints for further model development. In particular, these orbital distributions need to be accompanied by a clear understanding of the selection biases present in the observed distributions.

5.3.1 Adding Colors: *ugrizy* Photometry

Combining the orbits with color information accurate to $\sim 0.01 - 0.02$ magnitudes for a significant fraction of the objects allows for additional exploration of sub-populations and investigation of similarities among the different groups. This is complicated by the fact that LSST will not take simultaneous color measurements; observations in different filters will often be separated by at least 30 minutes. For slow rotators this will not be a significant problem, especially when combined with

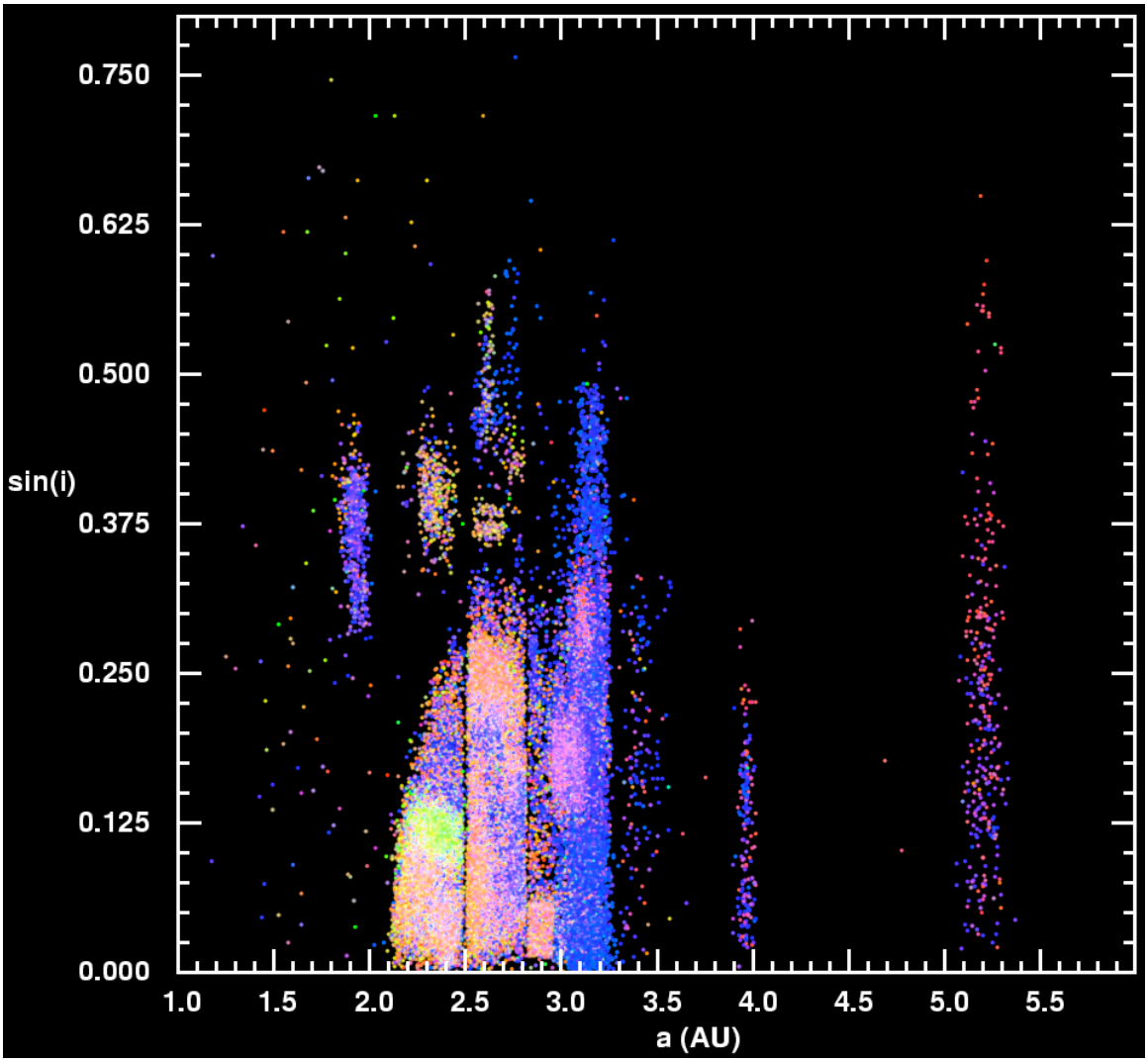

Figure 5.5: The dots show the sine of the osculating orbital inclination vs. orbital semi-major axis (a) distribution of $\sim$ 43,000 unique moving objects detected by the SDSS, and matched to objects with known orbital parameters. The dots are color-coded according to their colors measured by SDSS. About 1,000 Jovian Trojans are seen at $a \sim$ 5.2 AU, and display a correlation between the color and orbital inclination (Szabó et al. 2007). LSST will enable the construction of such a diagram with several million objects, including about 300,000 Jovian Trojans (50,000 with more than 150 detections).

many repeat measurements over the lifetime of the survey (however, it may increase the effective error in LSST color measurements).

This color information is useful in providing insights beyond the orbital distributions as shown in studying differences between the "hot" and "cold" classical Kuiper Belt. These two populations are just barely distinguishable by looking at the statistical distribution of inclinations of classical belt objects. However, the statistical color differences between the two groups are clear (Doressoundiram et al. 2008, 2005; Elliot et al. 2005), indicating a strong likelihood of significantly different dynamical histories, rather than just a bimodal distribution of inclinations. The colors of "cold"

(low inclination, low eccentricity) classical belt members tend to be only red, while the colors of "hot" (wider range of inclination and eccentricity) classical belt members range from red to gray. These differences are hard to explain with any of the current models of the outer Solar System, thus providing an important challenge for testing these and future models of the evolution of the Solar System.

As another example of the application of color data to understanding the history of small bodies, giant planet irregular satellites with a variety of inclinations show clear "families" when their orbital parameters are combined with color information (Grav et al. 2003; see Figure 5.6). With the addition of this information, the likelihood of different methods of capture mechanisms — gas drag capture of a series of small bodies versus capture of one parent body which was then broken apart through tidal stresses or collisions — can be evaluated.

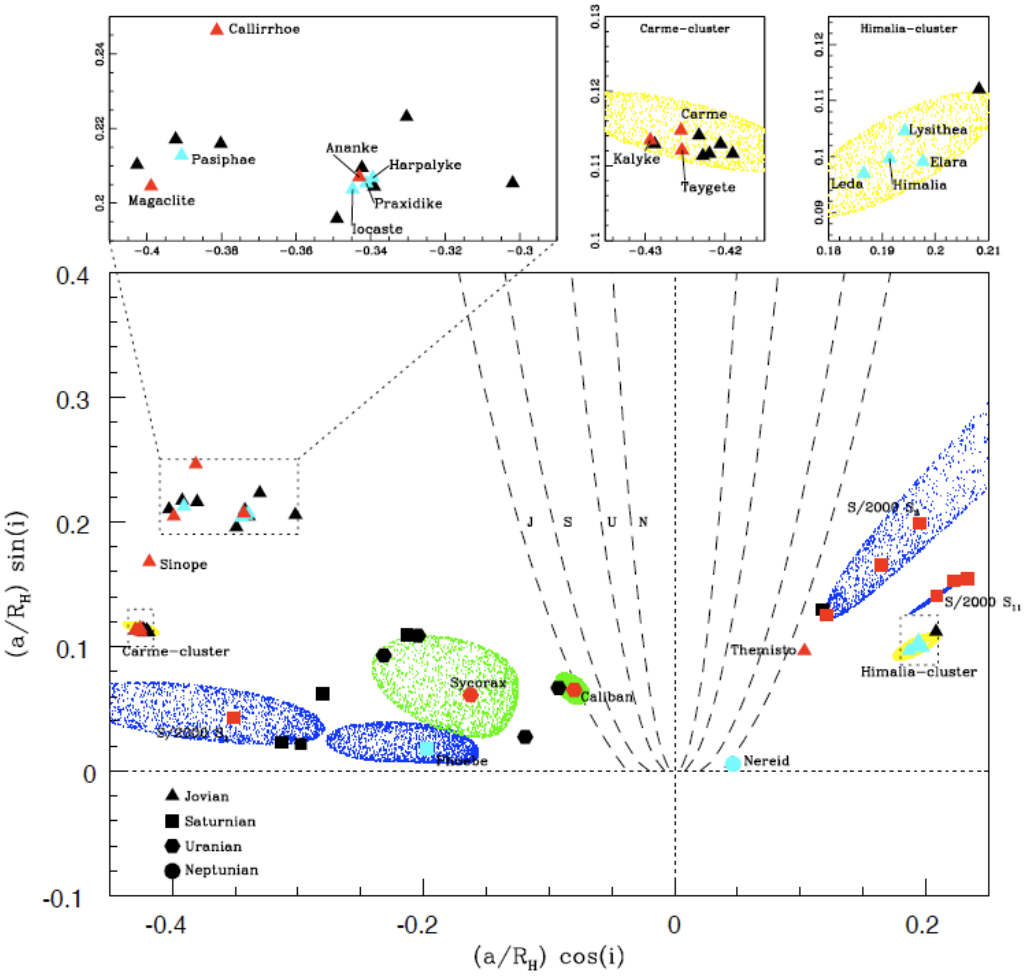

Figure 5.6: Distribution of irregular satellites around the giant planets. The x-axis is the component of the distance of the semi-major axis of each satellite along the axis of rotation of the planet, normalized by the planet's Hill-sphere radius; the y-axis is the component perpendicular to the axis. Irregular satellites with measured colors have been binned into "gray" or "red" color bins and are plotted according to blue for "gray" objects and red for "red." The colored ellipses indicate the area of $a - i$ space where each cluster could disperse, given a catastrophic fragmentation event. From Grav et al. (2003), with permission.

5.4 The Main Belt: Collisional Families and Size Distributions

Due to its large intrinsic and nearby (thus bright) population, the Main Asteroid Belt has historically provided the largest observational samples of small body populations. The size and color distributions of the Main Belt signal the history of individual bodies and their place within the larger population, providing clues to their history of accretion and collisional disruption. It is necessary to understand the role collisions and accretion play within each population if we are to understand planetary formation in detail.

5.4.1 Identifying Collisional Families in the Main Belt

Zoran Knežević, Andrea Milani

Collisional families provide constraints on all parameters appearing in evolutionary theories of small body populations: collision frequency and mean lifetime between disruptions, material strength of the bodies, timescales of dynamical diffusion due to chaos, secular resonances and non-gravitational perturbations, space weathering of surfaces, evolution of multiple systems, and rotation states. LSST is more likely to discover statistically significant numbers of collisional families (and their members) in the Main Belt rather than in the Kuiper Belt, due to the lower ratio of velocity dispersion (among the family members) to relative velocities (compared to non-family members).

The primary requirement for identifying collisional families in the Main Belt is obtaining accurate proper orbital elements for all objects which are "regular" or at least in stable chaos. Orbital elements calculated from observations are "osculating elements" – most reported orbital elements are osculating elements. "Proper elements" can be computed, starting from the osculating elements, in different ways: a typical method is to integrate the osculating orbital elements forward over a long time scale, averaging the osculating elements to calculate proper elements. The distinctive property of proper elements is that they are nearly constant over very long time scales, thus a similarity of the orbits is preserved for the same time span.

The algorithms to compute proper orbital elements depend on the orbital region of the object. In the Main Asteroid Belt, proper elements are stable for time spans between a few times 10^6 and a few times 10^8 years. If a catastrophic disruption event occurred even a very long time ago, the proper elements show clustering. These clusterings can be identified because the ejection velocities of the fragments, which are of the order of the escape velocity from the parent body, are smaller than the orbital velocities by two orders of magnitude. The ratio increases as catalogs reach smaller sizes of bodies.

The processing load for the computation of proper elements is expected to be quite significant for LSST's expected rate of discovery. Sophisticated tools of parallel computing are being developed to calculate proper elements. Development is ongoing in identifying clustered groups of objects within a denser background. The main families within each orbital region can be identified, using only comparatively large objects to avoid the chaining effects which prevent the use of currently known mathematical taxonomy methods for overly dense samples. Thus "core families" with larger objects can be formed with well tested methods, such as hierarchical clustering with the nearest neighbor metric. Given these defined families, the smaller objects can be tested for classification into potential families within their same orbital region. There is unavoidably some potential for

objects being classified in more than one family, the removal of this ambiguity can be obtained, at least partially, by using multicolor photometry.

Adding information about the photometric colors can aid in identifying families, as objects coming from the same parent body might be expected to have similar colors. The most striking example of this is the Vesta family, which is too large (also as a result of non-gravitational perturbations) to be discriminated by proper elements only, but is characterized by a very distinctive spectral signature. It should be noted that this is only an aid in identifying some potential families; if the parent object was differentiated and then completely disrupted, the family members could have very different spectral signatures (and thus colors) depending on their point of origin in the parent body.

The families act as a probe of the orbital stability of their members, taking into account both conservative chaotic diffusion and non-gravitational perturbations such as the Yarkovsky effect. The instability gaps and leaks detected in the families should be investigated for their dynamical mechanism and long-term evolution. They allow one to estimate the age of the families, as with the Veritas family, and to constrain physical properties such as thermal conductivity. Combined with the sparse light curve inversion, which should allow the determination of the rotation axis, the family member leakage could be used to validate and constrain Yarkovsky effect models. Another method to estimate the family age uses the distribution of proper semi-major axis as a function of absolute magnitude and thus size.

Individual objects break up due to collisions, tidal and rotational instabilities, and possibly other causes. A goal for future work is to identify recent and small events, as opposed to the large and ancient (millions of years) disruptions documented by the families. It is necessary to use very accurate proper elements in combination with direct numeric and semi-analytic computations to find and analyze such cases. Very recent breakups could belong to two categories: disruption of a binary into a two-component family or collisional catastrophic disruption of small bodies. Very recent collisional breakups with ages of the order of a million years are already known, and their number should increase very significantly by increasing the inventory of small objects.

There is an excess of pairs of asteroids on very similar orbits that indicates a common origin between the paired objects. Given the extremely low relative velocities (down to $< 1\,\mathrm{m\,s^{-1}}$), these cases appear most likely to be generated by fission of a solitary body or separation of binary components. Mapping the frequency, size distribution, and other properties of these pairs will provide constraints on the rate and nature of the fissions induced by tides and/or non-gravitational perturbations. With the single-visit limiting magnitude $r = 24.7$, LSST will produce a more complete catalog down to a given size range, which should increase the number of identified asteroid pairs enormously. This applies in particular to the Hungaria region, which is the subset of asteroids best observable from Earth in the context of a very large field of view survey such as LSST. Given the expected limiting magnitude of LSST, Hungaria family members with absolute magnitudes H up to 23 should be very well observable, and their number is expected to be comparable to the total number of MBAs presently known. Pairs with a primary of less than 500 m diameter, and a secondary around 200 m diameter should be found. This in turn will constrain the rate of formation and the stability of binary asteroids although most of them will not be directly observable with LSST.

5.4.2 The Size Distribution of Main Belt Asteroids

Željko Ivezić, Alex Parker, R. Lynne Jones

The size distribution of asteroids is one of most significant observational constraints on their history and is considered to be the "planetary holy grail" (Jedicke & Metcalfe 1998, and references therein). It is also one of the hardest quantities to determine observationally because of strong selection effects in the extant catalogs. Based on a comparison of recent known object catalogs (the ASTORB compilation of asteroid orbits from January 2008, Bowell 2009) and the SDSS Moving Object Catalog 4 (Ivezić et al. 2001), Parker et al. (2008) concluded that the former is complete to $r = 19.5$. LSST will produce a moving object catalog complete to a limit 5 magnitudes fainter.

Determining the size distribution of Main Belt Asteroids requires unraveling a complex combination of the background size distribution and varying size distributions of asteroid families. Asteroid dynamical families are identified as groups of asteroids in orbital element space (Gradie et al. 1979, 1989; Valsecchi et al. 1989). This clustering was first discovered by Hirayama (Hirayama 1918, for a review see Binzel 1994), who also proposed that families may be the remnants of parent bodies that broke into fragments. About half of all known asteroids are believed to belong to families; for example, Zappala et al. (1995) applied a hierarchical clustering method to a sample of 12,487 asteroids and found over 30 families.

Asteroid families are traditionally defined as clusters of objects in orbital parameter space, but SDSS data shows that they often have distinctive optical colors (Ivezić et al. 2002). Recently, Parker et al. (2008) studied the asteroid size distribution to a sub-km limit for Main Belt families using multi-color photometry obtained by SDSS. They showed that the separation of family members from background interlopers can be significantly improved with the aid of colors as a qualifier for family membership, although this method is not generally applicable for families resulting from the breakup of a differentiated parent body whose members could have significantly different colors.

Using a data set with $\sim$ 88,000 objects, they defined 37 statistically robust asteroid families with at least 100 members (see Figure 5.7). About 50% of objects in this data set belong to families, with the fraction increasing from about 35% to 60% as asteroid size drops below $\sim$ 25 km.

According to Parker et al. (2008), the size distribution varies significantly among families, and is typically different from the size distributions for background populations. The size distributions for 15 families display a well-defined change of slope and can be modeled as a "broken" double power-law (see Figure 5.8). These complex differences between size distributions probably depend on the collisional history of individual families and offer an observational tool to study the evolution of the Solar System.

The currently available data set is limited to $H \sim 15$, and includes several hundred thousand objects. The LSST data set will include several million objects, and will extend these studies to $H \sim 20$ (a limit ten times smaller, corresponding to about several hundred meters). In addition, over 150 detections will be available for about million objects (see § 5.2.4) enabling studies of asteroid rotation via light curve inversion, (see § 5.7) and providing exquisitely accurate colors for taxonomy. While taxonomy is not representative of composition, it can provide a first set of guidelines if spectra is not available.

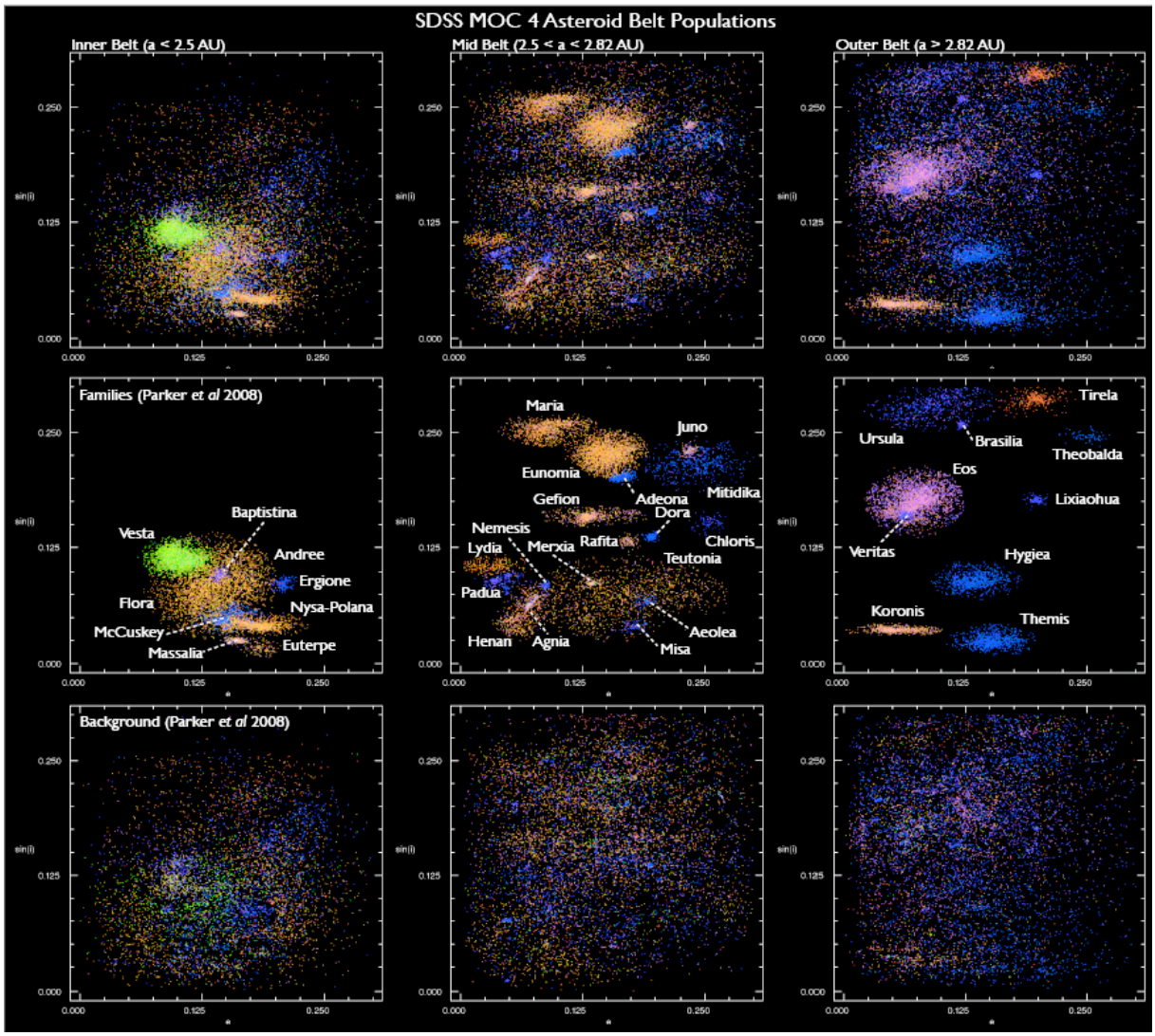

Figure 5.7: Illustration of the decomposition of the Main Belt asteroid population into families and background objects using proper orbital elements and color (adapted from Parker et al. 2008). The top three panels show the sine of the orbital inclination vs. orbital eccentricity diagrams for three regions of the Main Asteroid Belt defined by semi-major axis range (see the top labels). Each dot represents one object, and is color-coded according to its color measured by SDSS (see also Figure 5.5 for a "zoomed-out" view). The three middle panels show objects from 37 identified families, and the bottom three panels show the background population. Examples of size distributions for several families are shown in Figure 5.8. These results are based on about 88,000 objects. The LSST data set will include several million objects and will also provide exquisite time domain information.

Previous surveys have shown that the albedo distribution of asteroids is bimodal, with one peak having a mean albedo of 0.06 while the other peak has a mean of 0.20 in g or about 0.25 in r or i. These two different albedo peaks are correlated with asteroid color, representing their taxonomic types. Low albedo MBAs are C-, D-, and P-types asteroids, while those MBAs with higher albedos are S-, R-, V-, E-, and M-type asteroids.

LSST data can be used to measure MBA taxonomies, which may be used to constrain the albedos

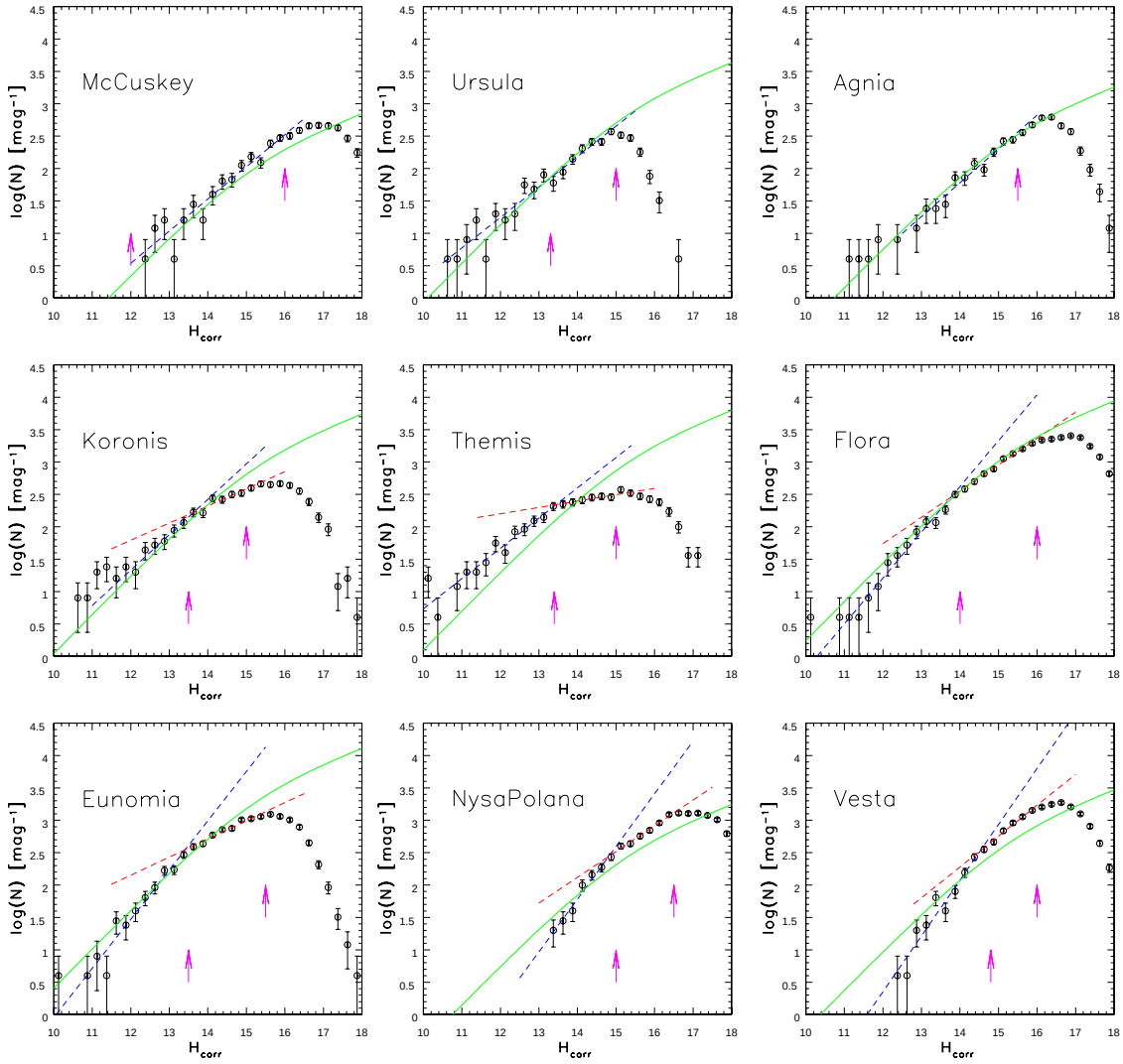

Figure 5.8: The differential absolute magnitude distributions from SDSS data for selected asteroid families (see Figure 5.7), shown as symbols with Poisson error bars (adapted from Parker et al. 2008). The green solid line in each panel shows the distribution for the whole Main Belt with amplitude fit to the data. The two dashed lines show the best-fit power-law fits for the bright (blue) and faint (red) ends separately. The two arrows show the best-fit break magnitude (left) and the adopted completeness limit (right). The current catalogs are limited to $H < 15$; the LSST data set will extend these studies to $H \sim 20$.

of the MBA population. However, it is important to note that asteroids of the same taxonomic type can have a wide range of compositions and albedos. In addition, asteroids of disparate compositions may appear to belong to the same taxonomic group, but have completely different albedo values. Hence any broad generalizations about the MBA population albedo distribution with respect to taxonomy should be made with the utmost of caution. Even with this caveat, the real power of the LSST photometry will be in its large number statistics, which may help in improving the size estimates of a large portion of the MBA population, perhaps improving the uncertainty on the size estimate from 30% – 50%.

5.4.3 Determining the Masses of Large Main Belt Asteroids

Steven R. Chesley, Zoran Knežević, Andrea Milani

While the size distribution is estimated from the photometric observations of color and absolute magnitude, one can also attempt to measure the masses of larger asteroids directly from the perturbation of other, typically smaller, "test particle" asteroids that pass near the perturber. At present only a few dozen asteroids have mass estimates based on perturbations, but LSST will produce astrometry that is both prolific and precise, at the same time that it dramatically expands the pool of potential test particles. LSST data should allow the estimation of the mass of several hundred or so main belt asteroids with an uncertainty of $\sim 30\%$ or less. These estimates will provide many more mass bulk density estimates than are currently known, constraining the internal structure and/or mineralogy of many asteroids. Moreover, asteroid mass uncertainty remains the largest source of error for precise asteroid (and planetary) ephemerides. Driving this uncertainty lower will afford more precise predictions of asteroid and planetary trajectories.

The main problem of this technique is the complexity of explicit, simultaneous computation of a large number of asteroid orbits; while the target objects for which the mass may be computed are few, the list of objects potentially having a close approach is on the order of millions. To avoid intractable computational complexity, the candidate couples need to be selected through a sequence of filters. After an elementary selection based on absolute magnitude, perihelia and aphelia, one of the filters is based on the computation of the Minimum Orbital Intersection Distance (MOID) between two asteroids; this computation can be refined by also taking into account the orbital uncertainties. If the MOID is small, the maximum amount of deflection can be computed from a two-body hyperbolic formula. Only when the result of these preliminary computations indicate the possibility of a measurable deflection, then an accurate orbit propagation for the smaller asteroid, including the larger asteroid in the dynamic model, needs to be performed. If the close approach actually occurs with an observable signal, for the given (or expected) set of observations, then actual orbit determination with mass as an additional fit parameter takes place (this both in simulated/predicted cases and in actual data processing).

5.5 Trans-Neptunian Families and Wide Binaries

Michael E. Brown, R. Lynne Jones, Alex Parker

Only one collisional family of objects is currently known in the outer Solar System. Haumea, the fourth largest object known beyond Neptune, orbits within a dynamical cloud of debris left over from a giant impact with a comparably-sized object (Brown et al. 2007). Such a giant impact is exceedingly improbable in the current environment, and even difficult to explain in a more dense earlier environment. Levison et al. (2008c) realized that collisions between objects being scattered by Neptune could potentially explain this family. This suggests that many collisional families should exist in the outer Solar System and their orbital distributions could trace the scattering history of the early Kuiper Belt.

The Haumea family was recognized only because each of its members shares the same distinct infrared spectrum: a surface dominated by almost pure water ice. Without the spectra, the family

could not have been recognized as no statistically significant concentration could be identified by dynamics alone (Figure 5.9). The icy surface of the family members is likely the result of the differentiation of proto-Haumea before impact, where the family members are pieces of the pure ice mantle. As there are strongly identifiable spectral features associated with only a few TNOs, other collisional families in the Kuiper Belt cannot currently be identified by their spectra, but rather will have to be identified as significant concentrations in dynamical space, as the asteroid families are identified. Such identification may be possible with LSST due to the large number of TNOs discovered with well-measured orbits, and will be aided by information on colors and perhaps other physical properties (such as rotation rate).

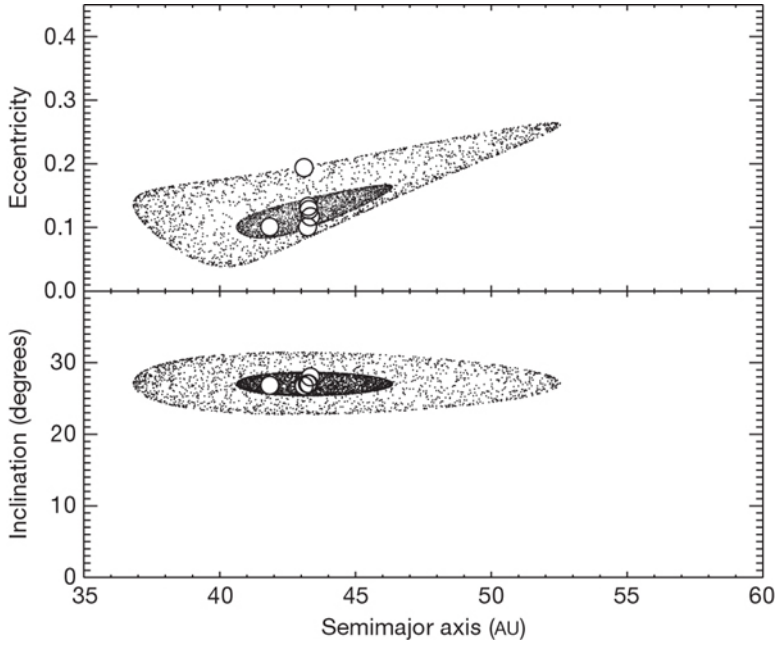

Figure 5.9: Figure from Brown et al. (2007). The open circles give the proper orbital elements of the KBOs thought to be part of a collisional family with Haumea. The widely dispersed small dots show the orbital elements possible from a collision centered on the average position of the fragments and with a dispersive velocity of 400 $\mathrm{m\,s^{-1}}$. The more tightly concentrated dots show orbital elements expected if the collision had a dispersive velocity of 140 $\mathrm{m\,s^{-1}}$. The orbital dispersion from these collisions indicates that identifying collisional families in the Kuiper Belt will require accurate orbital elements for a large number of objects and may be strongly aided by color or other physical measurements.

Along with collisional families, Kuiper Belt binaries offer a unique window into understanding the physical structure and composition of TNOs. Accurate mutual orbits allow determination of component masses and, if coupled with size measurements derived from thermal observations or direct detection, densities. The ice-to-rock fraction of objects in the Kuiper Belt is not constrained other than in the Pluto-Charon system, but is a strong indicator of the chemical environment at the time of formation (Lunine 1993). Density measurements are therefore essential in establishing the composition in the early solar nebula, similar in importance to the compositional gradient observed in the Main Belt of asteroids.

Binarity in the Kuiper Belt looks distinctly different than that in the Main Belt: known TNO binaries are likely to be widely separated and roughly equal mass. Among NEAs and small MBAs,

binaries tend to be closely bound with the primary rapidly spinning, suggesting that they have formed by fission, perhaps due to over-spinning of a single body by the YORP radiation torque as described below in § 5.7.1. Widely separated binaries of nearly equal-sized bodies suggest completely different formation mechanisms, and as a result of the different evolutionary history in the Main Belt compared to the Kuiper Belt, most resolved binary systems detected by LSST will be wide TNO binaries.

A number of theories describe the formation of TNO binaries, and to some degree offer testable predictions. In the early dense environment, satellites can be captured by the effects of dynamical friction (Goldreich et al. 2002), through two-body collisions, or exchange reactions in the presence of a third planetesimal (Weidenschilling 2002; Funato et al. 2004). Large Kuiper Belt objects appear to have tiny satellites formed as a result of giant impacts (Brown et al. 2006), which may be related to yet-unidentified collisional families. Each of these processes preserves traces of the environments of the regions where the objects formed, which are likely dramatically different from the current Kuiper Belt environment, where low interaction rates among TNOs make forming binaries extremely unlikely.

Work with the Hubble Space Telescope (HST) has shown that the cold classical Kuiper Belt has a significantly higher fraction of resolved satellites than any other TNO population: 22% rather than 5.5% (Noll et al. 2008). However, the sample of known binaries is small. LSST, in the course of detecting $> 20,000$ TNOs, will also find many satellites ($\sim 50 - 100$) separated by arcseconds, allowing detailed study of these systems. Measuring the statistical properties of the large-separation binary orbit distribution, which are most sensitive to disruption and formation mechanisms, will tell us which mechanism(s) were at work, provide constraints on the dynamical history and space densities of the Kuiper Belt, and help us understand how those objects survived until present time in the disruptive dynamical environment of the Kuiper Belt.

5.6 The Size Distribution for Faint Objects—"Shift and Stack"

Steven R. Chesley, R. Lynne Jones, David E. Trilling

In addition to measuring the size distribution through a near complete inventory of larger objects, LSST can extend the size distribution estimate to much smaller sizes through a special program of deep fields (§ 2.1), capitalizing on the large LSST aperture and quick CCD read-out times to search for very faint TNOs, Trojans, MBAs, and potentially even NEAs.

The strategy for such an LSST "deep drilling" project is to maintain a given pointing for successive exposures until the desired depth can be obtained in a sum, or "stack," of all images. For routine follow up and recovery work the individual images are stacked with the known rate of motion of the target body, but for initial discovery with LSST deep fields, a family of stacks is necessary to cover the range of motion vectors for each of the target populations. The large number of stacks, in the thousands for MBAs, leads to a non-trivial computational problem, with the challenge proportional to the time duration of the stack, since more stacking rates are required to avoid trailing of a given target in at least one of the stacks. Thus single night stacks are significantly more attractive than multi-night stacks.

As an example, LSST will be able to track a single opposition field for up to eight hours in winter, during which time it could obtain about 850 "single-visit" exposures of 30 seconds each. Since the signal-to-noise ratio for N exposures follows $\sqrt{N}$, the stack from these images will reveal detections about 3.7 magnitudes fainter than the single visit $5\,\sigma$ limit of $r = 24.7$. However, $7\,\sigma$ limits are generally more appropriate for detections in deep stacks, and so we estimate that a single night stack will reach $r \approx 28.0$. This translates to diameters more than 5 times smaller than the single visit limit. To reach this limiting magnitude, stacking will have to be done with a few thousand different assumed rates, the vast majority being at main belt rates. All observations would be carried out in the same filter—probably r. Potentially, exposure times other than 30 seconds would be explored for this mode of operation to reduce the number of images required to shift and stack.

The first epoch is repeated at a later time, ideally on the next night so that more than 90% of MBAs will remain in the field, which, for opposition fields, is generally sufficient to obtain a reliable topocentric distance and hence absolute magnitude. For TNOs, the field should be repeated a few months later when it is at a significantly lower solar elongation. In that case, it may take two partial nights of staring to reach the desired limiting magnitude, since the field is not observable the entire night. However, the stacking requirements for TNOs are much less demanding (they move much more slowly!), and so multi-night stacking appears tractable. At a cost of 1-2% of survey time, this three-night deep-drilling cadence process could be repeated annually on the same field for a few years, building up a large set of MBA detections and solidifying the orbits of the TNOs in the field.

The deep TNO survey should have several unique pointings overall. In consultation with other science drivers, these should be divided between ecliptic and off-ecliptic pointings. The ecliptic pointings—at various ecliptic longitudes—would allow a longitudinal probe of the outer Solar System small body population. This is particularly important since the sky density membership of resonant objects – a key probe of outer Solar System evolution – varies as a function of ecliptic latitude and longitude. The off-ecliptic pointings would provide a three-dimensional map of the outer Solar System down to very small sizes. It is worth noting that other science drivers would profit from the same deep stack data sets.

Deep drilling fields targeting the outer Solar System could profitably also include the Trojan clouds of Jupiter and Neptune (as well as hypothesized Trojan clouds of Saturn and Uranus, though no Trojan asteroids for these planets are currently known). Jupiter and Neptune are in conjunction in mid-2022, and so their leading and trailing Trojan clouds will be respectively aligned at this time, making it a good opportunity to probe the Trojan populations of both planets—in addition to MBAs and TNOs—with a minimum of telescope time. About four years earlier, in 2018, the leading Jupiter cloud coincides with the trailing Neptune cloud, forming another good opportunity.

The deepest search for TNOs to date reached $r \sim 29$ over 0.02 deg^2, obtained with HST/ACS (Bernstein et al. 2004). Thus, a deep drilling experiment with even a single LSST field will increase the areal coverage by a factor of ~ 500. Using the Bernstein et al. (2004) result to predict LSST results at $r \sim 28$, we expect something like 1000 TNOs per deep drilling field on the ecliptic; off-ecliptic fields may have densities one tenth this value. For MBAs, each deep field should yields upwards of 20,000 detections.

Successfully detecting faint ($r \sim 28$) MBAs enables science in a different size regime than the projects described in § 5.4.2. For example, the size distribution of MBAs is known to have significant structure that records the intrinsic strength of asteroids (e.g., O'Brien & Greenberg 2005), and probing to this size regime will allow studies of the global internal properties of asteroids. Additionally, small MBAs are the direct predecessors of NEAs (that is, the sizes of typical NEAs are comparable to those of "very small" MBAs that are only available through an LSST-type deep drilling project as described in § 2.1). Therefore, by measuring the properties of very small MBAs (i.e., size distribution, orbital distribution), we can probe the links and processes by which MBAs become NEAs. A study of the MBA-NEA connection is only possible with both an NEA survey *and* a very deep MBA survey such as described here. This link between the two is described further in § 5.8.1.

5.6.1 Detection of Extremely Faint Objects through Real-Time Collisions

R. Jedicke

We will measure or set a limit on the collision rate of MBAs too small to detect directly with LSST. We will do this by searching for signatures of the transient dust clouds produced in the catastrophic collision of two objects that are otherwise too small to detect, or by detecting transient increases in the brightness of asteroids. This will allow us to

- test whether the size–frequency distribution (SFD) measured for the larger Main Belt objects can be extrapolated to smaller sizes,
- test and refine collisional models, and
- understand the physical structure of asteroids.

There is expected to be roughly one catastrophic disruption of a 10 m diameter main belt object every day and, given LSST's sky coverage, we expect to image about one of these disruptions every week. As the dust cloud from a catastrophic disruption expands, its apparent brightness increases as long as the optical depth $\tau > 1$ after which the clouds brightness will decrease. A 10 m diameter asteroid's disruption could create a dust cloud 1 km in diameter which would have the apparent brightness of a 1 km diameter asteroid (easily detected by LSST).

The difficulty lies in knowing the expansion rate of the dust cloud and therefore determining how long the cloud is visible. If the cloud is visible for many days to a week we might detect the expanding dust cloud on each of three nights during a lunation. The brightness of the cloud could vary dramatically from night to night, and it will be impossible to recover the object or assign a detection to a previously detected object. If the dust cloud does not last that long it is possible that we will detect bright but 'orphaned' tracklets that are impossible to link to other tracklets.

It may also be possible to detect the collision of small objects into larger objects that are easily detected by LSST. By continuously monitoring many objects over the LSST operational lifetime we can search for unusual and unrepeated brightening of asteroids as a signature of a recent collision.

With a sufficient number of collisions we may determine the collision rate of these objects. The rate at which the dust clouds brighten and fade will provide details on the physical structure of the asteroids. Color measurements or detailed spectroscopic followup of the dust clouds will provide

information on the dust properties. If the collisions produce enough large grains, the clouds may be observable in the infrared for much longer if followup could be obtained from space.

5.7 Lightcurves: Time Variability

Stephen T. Ridgway, R. Lynne Jones

The variation in the apparent brightness of solid Solar System bodies can be a valuable source of information about their history, their surfaces and even their interiors. Cyclic variations can show the rotational period and rotational axis orientation, the shape, compositional clues, the density, and information about the surface roughness. Many objects have brightness variations on the order of only 0.2 magnitudes, and require accurate, well sampled light curves for unambiguous interpretation. LSST will provide outstanding period coverage through the method of sparse light-curve inversion.

Asteroidal rotation and the direction of its spin axis are an obvious consequence of the accretion and collision process. Photometry can provide periods, and in some cases the spin axis can be estimated by the timing of brightness extrema (Taylor & Tedesco 1983). On the order of a few thousand asteroids have reliably measured rotation rates – Harris & Pravec (2006) provide a brief overview on asteroid rotational periods, which range from 2 hours up to about a day, reflecting tensile strengths and rubble pile or monolithic structures. Kryszczyńska et al. (2007) point to an online catalog of asteroid spin states and pole positions, illustrating a non-random distribution of pole axis positions likely due to radiation pressure torques. Some fraction of the asteroids will have detectable rotational lightcurves, which will allow determination of their rotational periods.

The amplitude of a rotational light curve can give a measure of the object shape, commonly modeled as a triaxial ellipsoidal. Contact or small separation (unresolved) binaries can be inferred from characteristic brightness variations, or in some cases, eclipses. Observed brightness variations may not be due entirely to object shape, but may also depend on varying albedo associated with compositional variations across the surface. Multicolor measurements can support separation of these effects, thanks to the known colors of a number of surface compositions – mineral or carbonaceous materials, or in the outer Solar System, ices. The albedo and apparent brightness then support a reliable estimate of object size. For rapidly rotating objects, the size gives a lower limit to the mass consistent with a rubble structure. Even for unresolved binary objects, the orbital period gives a dynamical measurement of the masses. Mass and size provide a measure of the densities, which constrain the ratio of minerals to ices and the porosity of the object. Kaasalainen & Torppa (2001) and Kaasalainen et al. (2001) have shown that several hundred accurate phase data are sufficient to support optimal inversion of lightcurves to determine shape and albedo distributions (see § 5.7.1 for more information).

To date, even after painstaking work, little is known about rotations of objects in the outer Solar System (Sheppard et al. 2008). At present, to measure a rotation, each object must be individually tracked and monitored with a large telescope for hours or days. Some rotations show up easily on these time scales, some are heavily aliased or too subtle for detection and the current sample of objects with known rotation periods is small. Nonetheless, a few interesting objects stand out. The large objects Varuna and Haumea have extremely rapid rotations (six and four hours respectively),

which cause them to elongate into triaxial ellipsoids (Lacerda & Jewitt 2007). Haumea is suspected to have suffered a family-producing collision, which likely imparted the spin. No such family has yet been dynamically linked to Varuna. Observations of rotations have suggested with poor statistics that a large fraction of objects could be contact binaries (Sheppard & Jewitt 2004). Such contact binaries could be a natural consequence of the dynamical-friction induced capture in the early Solar System (Goldreich et al. 2002) if the dense-early environment persisted for long periods of time allowing orbits of captured satellites to decay.

Small bodies do not normally reflect as Lambertian surfaces owing to shadowing in the surface microstructure. Thus the asteroid magnitude system employs two numbers to represent the brightness: a mean (normalized) magnitude, H, and also a phase factor, G, that describes the observed brightness variation as a function of the scattering angle. More detailed models attempt to relate the phase effect to the surface microstructure. LSST photometry will provide a massive body of homogeneously obtained phase data for on the order of a million asteroids (see § 5.2.4). Measurements at very small phase angles ($< 2^\circ$) are particularly valuable (Domingue & Hapke 1989), and while LSST will observe most of these asteroids near opposition as a matter of regular operations, additional follow-up targeted measurements could be scheduled at other facilities.

5.7.1 Sparse lightcurve inversion

Josef Ďurech, Mikko Kaasalainen

LSST will provide us with accurate photometry of a large number of asteroids. As has been suggested by many simulations (Kaasalainen 2004; Durech et al. 2005, 2007), this so-called "sparse photometry" can be used the same way as standard dense lightcurves to derive basic physical parameters of observed asteroids: the global shape, the spin axis direction, and the rotation period. Simulations that have been done so far showed that, roughly speaking, once we have at least ~ 100 sparse brightness measurements of an asteroid over ~ 5 years calibrated with a photometric accuracy of $\sim 5\%$ or better, a coarse model can be derived. This approach is much more time-efficient than the usual lightcurve photometry. The sparse data inversion gives correct results also for fast ($0.2 - 2$ h) and slow (> 24 h) rotators, although it may give best results with large amplitude variations and moderate periods.

As can be seen in Figure 5.4 the number of observations of individual asteroids is generally sufficient for lightcurve inversion. The median number of expected LSST detections over 10 years is ~ 190 for NEAs with $H \leq 15$ mag and ~ 260 for MBAs with $H \leq 16$ mag.

An important issue is to use all available data, so we will combine LSST sparse photometry with sparse and dense data from other sources (e.g., Pan-STARRS, follow-up observations, existing databases, etc.). Photometry can be also combined with adaptive optics images (Marchis et al. 2006) and occultation profiles to obtain more detailed models with accurate dimensions.

We expect to derive about 10^4 to 10^5 Main Belt and Near-Earth Asteroid shape models from LSST photometry, which means that we will be able to map a substantial part of the asteroid population. This will bring new insights into its structure, history, and evolution. We will be able to detect Yarkovsky and Yarkovsky-Radzievskii-O'Keefe-Paddock (YORP) effects that can secularly change orbits and spins of asteroids. Both effects are caused by the anisotropic thermal

emission of the heated surface. While the Yarkovsky effect describes the change of the orbit caused by the net thermal force, the YORP effect describes the influence of the thermal net torque on the spin state (see Bottke et al. 2006 for a review). The distribution of spin rates and obliquities will allow us to quantify the YORP evolution. We also expect to reveal new populations in spin-orbit resonances (Vokrouhlický et al. 2003). In addition, by constraining the Yarkovsky effect, this would be potentially very important in discerning the history of genetic pairs.

For TNOs, the viewing/illumination geometry changes very slowly and the full solution of the inverse problem is not possible. However, accurate sparse photometry can be used for period determination.

Due to the stability and uniqueness properties of the inverse problem solution derived from the disk-integrated photometry, asteroids are mostly modeled as convex bodies. LSST sparse photometry can be also used for detecting (but not modeling) "non-standard" cases such as binary and tumbling asteroids. A fully synchronous binary system behaves like a single body from the photometric point of view (Durech & Kaasalainen 2003). Its binary nature can be revealed by the rectangular pole-on silhouette and/or large planar areas of the convex model. In some cases – when mutual events are deep enough – asynchronous binaries can be detected from sparse photometry. Interesting objects can then be targeted for follow-up observations.

5.8 Overlapping Populations

As we discover and characterize more small bodies throughout the Solar System, more surprises are uncovered. One such area is the discovery of linkages and overlaps between different populations of objects. The discovery of asteroids showing cometary activity is an example of the overlap of physical properties between different populations. Simulations demonstrating that objects can have orbits which slowly cycle between the inner Oort Cloud and the Scattered Disk or even Centaur regions, or from the MBAs into NEA orbits, imply that to fully understand each of these groups requires understanding the Solar System as a whole.

5.8.1 The Relationship between NEAs and MBAs

Alan W. Harris, Steven R. Chesley, Yanga R. Fernández, R. Lynne Jones

Orbits crossing the orbits of the giant planets have lifetimes of only thousands of years; those crossing the terrestrial planets have lifetimes of millions of years, which is still short enough that none of the current population of NEAs is "primordial" in their current orbits. Their dynamical lifetimes are only on the order of 10^6 to 10^8 years due to interactions with other objects in the inner Solar System that cause them to either impact one of the inner planets or the Sun, or be ejected from the Solar System altogether (Morbidelli & Gladman 1998). Hence the continued presence of these objects within near-Earth space requires a mechanism(s) and source region(s) to replenish and maintain the NEA population over time.

Current dynamical models and orbit integrations (Bottke et al. 2002) suggest that NEAs are delivered primarily from specific regions within the Main Belt that are particularly affected by certain secular and mean-motion resonances. However the Yarkovsky effect can push objects from

different parts of the Main Belt into orbits that make them more likely to be thrown inward. Therefore it is crucial to study the migration within the Main Belt if we are to learn where NEA material comes from.

A key to understanding the transfer of MBAs into near-Earth orbital space is to determine the population of both classes, especially in the same size range. Presently, we only know the size frequency distribution (SFD) of MBAs down to a size of several km diameter. Unfortunately, only the largest hundred or so NEAs are that large, so there is very little overlap of our measured SFD of NEAs with that of MBAs. LSST will extend that overlap down to sizes of ~ 100 meters diameter in the Main Belt, providing enough overlap to examine the differences of the SFDs. This will shed light on the efficiency of migration into Earth-crossing orbits versus size, or whether close planetary encounters modify the distribution, say by tidal disruptions, and the effect that Yarkovsky and YORP have in these transfer mechanisms.

By the time LSST begins operations in 2014, nearly all of the NEAs with diameters greater than 1 km will have been cataloged by surveys such as Pan-STARRS. At smaller sizes, down to perhaps 150m, LSST, over its lifetime, will discover and catalog nearly all ($\sim 90\%$) of the NEAs. In the size ranges where nearly all of the NEAs have been discovered, the orbits of each asteroid can be propagated forward to determine the probability of future impacts with the Earth and the Moon. At sizes smaller than that at which the catalog is complete, characterizing the future impact hazard will remain a statistical problem of estimating size frequency distributions and orbital distributions from a limited sample of objects. At these smaller sizes, a statistical description of the size frequency distribution and orbital distribution along with taxonomic identifications can yield insight into the source regions that resupply the NEAs and whether the resupply processes differ by size. There is also utility in characterizing the past impact flux on the Earth, the Moon, and other bodies, in comparison with the cratering record, to understand whether and how impact fluxes have changed over the history of the Solar System.

5.8.2 Damocloids and Main Belt Comets: Asteroids on Cometary Orbits and Comets on Asteroidal Orbits

Paul A. Abell, Yanga R. Fernández

The Main Belt asteroids have been recognized as one of the primary sources of material for the NEA population (McFadden et al. 1985), but several investigators have suggested that a non-negligible portion of the NEA population could also be replenished by cometary nuclei that have evolved dynamically into the inner Solar System from such reservoirs as the Edgeworth-Kuiper Belt and the Oort Cloud (Weissman et al. 2002). Evidence used to support the hypothesis of a cometary component to the NEA population has been based on: observations of asteroid orbits and associated meteor showers (e.g., 3200 Phaethon and the Geminid meteor shower); low activity of short-period comet nuclei, which implied nonvolatile surface crusts (e.g., 28P/Neujmin 1, 49P/Arend-Rigaux); lack of recent cometary activity in NEAs observed to have apparent transient cometary activity in the past (e.g., 4015 Wilson-Harrington); and a similarity of albedos among cometary nuclei and asteroids in comet-like orbits. Recent studies have estimated that approximately 5 – 10% of the entire NEA population may be extinct comets (Fernández et al. 2005; DeMeo & Binzel 2008).

Thus several observational investigations have focused on examining low-activity short period comets or asteroids in apparent comet-like orbits. A population that has been thought to have probable connections to the Oort Cloud and the isotropic comets are the Damocloid asteroids. The Damocloid-class objects are thought to be possible dormant or extinct comets because these asteroids have high-inclinations and large semi-major axes just like those of Halley-family and long-period comets (Asher et al. 1994; Bailey & Emel'Yanenko 1996). About 50 such objects are known (as of Sept 2009), although all of the objects so far seem to have evolved orbits. That is, none of the objects is new in the Oort sense. Most observations of these objects suggest that they have similar spectral characteristics to those of Jupiter-family comets and outer Main Belt asteroids, but show no evidence of coma (Jewitt 2005). However, at least one Damocloid object (C/2001 OG_{108}) demonstrated intense coma during its perihelion passage 1 AU from the Sun after showing no coma for several months beforehand, which supports the notion that Damocloids in general could be dynamically evolved objects from the Oort Cloud (Abell et al. 2005).

In addition, it seems that the conventional dynamical and physical demarcation between asteroids and comets is becoming even less clear. Observations of a few objects located within the Main Belt asteroid population show degrees of activity that are normally a characteristic of cometary objects (Hsieh & Jewitt 2006). Dynamical modeling of the dust generated from these Main Belt objects suggests that this level of activity requires a sustained source, and is not the result of impulsive collisions. Thus it is plausible that an additional cometary reservoir exists within the Solar System among the main belt asteroids (Hsieh & Jewitt 2006). If these objects were formed in-situ, they would suggest that condensed water ice survived to the present-day much closer than traditionally believed. However there could be dynamical mechanisms that can place outer Solar System objects into low-eccentricity, outer Main Belt orbits (Levison et al. 2008a), so the origin of these objects is an important science question. Only four such main belt comets (MBCs) have been discovered to date, but given the low level of activity in these objects, many more could be present below the current detection limits of existing ground-based sensors.

During survey operations, the LSST will discover many more low albedo Damocloid objects, and have the capability to detect faint/transient activity from MBC candidates. A large statistical database of several hundred Damocloids and MBCs would be an invaluable resource for understanding volatile distribution in the Solar System and thermal evolution of small bodies. In addition, objects originating in the different cometary reservoirs (Oort Cloud, Edgeworth-Kuiper Belt, and potentially the Main Belt) may have distinct physical characteristics. LSST will not only be the optimal system for discovering a majority of these objects, but will let us use gross physical properties (e.g., lightcurve, colors, taxonomy, etc.) to make comparisons across many Solar System populations at different stages of their evolution. This will enable investigators to get a much clearer picture of these enigmatic Damocloid and MBC populations as a whole, which in turn will aid in the refinement of Solar System formation models.

5.8.3 The Source(s) of Centaurs

Nathan A. Kaib

Identifying the source population for Centaurs, which are similar in dynamical properties to Scattered Disk Objects but have orbits which cross interior to Neptune and are unstable over the

lifetime of the Solar System, has proven difficult. The generally accepted source region for Centaurs is the Scattered Disk. As SDOs chaotically diffuse into Neptune-crossing orbits on Gyr timescales, they naturally produce a population of unstable planet-crossers qualitatively similar to observed Centaurs. However, due to perturbations from passing stars and the Galactic tide, the Oort Cloud also steadily injects bodies into planet-crossing orbits. Because the Oort Cloud has a much higher typical semi-major axis than the Scattered Disk, objects with an Oort Cloud origin will dominate the high-a range of Centaurs, whereas objects from the Scattered Disk will dominate the low-a population of Centaurs (Kaib et al. 2009). However, energy kicks from planetary encounters will act to smear these two a-distributions leading to an Oort Cloud contribution even for Centaurs with semi-major axes less than that of the actual Oort Cloud.

With a semi-major axis of 796 AU, 2006 SQ_{372} was recently shown to have the highest probability of an Oort Cloud origin for any known Centaur (Kaib et al. 2009). Even using a conservative estimate for the total population of Oort Cloud objects, it was shown that this body is 16 times more likely to originate from the Oort Cloud compared to the Scattered Disk. Furthermore, the same analysis showed another known centaur, 2000 OO_{67} is 14 times as likely to come from the Oort Cloud as from the Scattered Disk. Even more intriguingly, dynamical modeling of these objects' production shows that they almost exclusively come from the inner 10^4 AU of the Oort Cloud. Known LPCs only provide an upper limit on the population of objects in this region and provide no constraints on the actual radial distribution of material in the Oort Cloud (Kaib & Quinn 2009), which is intimately linked to the Sun's formation environment (Fernandez 1997). Any additional constraints on this reservoir would be highly valuable. Although little information can be gleaned from only the two currently known objects of 2000 OO_{67} and 2006 SQ_{372}, LSST will have nearly 100 times the sky coverage of the survey that detected 2006_{372}. LSST will also be able to detect objects 4 magnitudes fainter as well. As a result, it is reasonable to expect LSST to discover a hundreds to thousands of objects analogous to 2006 SQ_{372}. Studying the orbital distributions of a large sample of these types of bodies will be able to further constrain the population size and provide the first constraints on the radial distribution of objects in the Oort Cloud.

5.8.4 The Source(s) of Comet Families

Yanga R. Fernández

The conventional idea is that Halley Family comets (HFC) and Long Period comets (LPC) originate from the Oort Cloud. However, dynamical modeling finds this very challenging to reconcile with current theories about the state of the Oort Cloud (see e.g., Duncan 2008). The difficulty lies in determining what structural differences there are (if any) between the inner and outer Oort Clouds, and how the physical aging and fading of HFCs and LPCs changes the population over time from what is injected into the inner Solar System to what we observe today. There is also a hypothesis that the Scattered Disk is responsible for some of the HFCs (Levison et al. 2006), which is interesting in light of recent compositional studies showing that there is more overlap in parent-molecule abundance between Jupiter Family Comets (JFCs) and LPCs than previously thought (Disanti & Mumma 2008). LSST will be able to address this situation by dramatically improving the number of HFCs and LPCs that are known. In particular, astrometry of LPCs while they are far from the Sun will make it easier to identify those that are new in the Oort sense (i.e., on their first trip in from the Oort Cloud) more quickly. The orbital elements of the HFCs and

LPCs will give us a less biased view of the current distribution of these comets in our Solar System, thereby constraining the dynamical models.

5.9 Physical Properties of Comets

Yanga R. Fernández

Comets are the most pristine observable remnants left over from the era of planet formation in our Solar System. As such, their composition and structure can in principle tell us much about the chemical and thermophysical conditions of our protoplanetary disk. This can then be used to understand the place of our Solar System in the wider context of planetary disks throughout our Galaxy.

Achieving this understanding of the protoplanetary disk using comets requires determining the evolutionary processes that have affected the comets we see today. In the 4.5 Gyr since formation, and even before the comets felt significant insolation by traveling into the inner Solar System, they suffered various processes – e.g., collisions, cosmic-ray bombardment, flash heating by nearby supernovae – that changed their physical and chemical properties from the primordial. It is crucial to understand evolutionary processes of small bodies in order to interpret what they may tell us about planetary formation. While this applies to all small bodies throughout the Solar System, it is particularly interesting in the case of comets (and especially comets inbound from the Oort Cloud for the first time) because they may be closer to the primordial state.

Currently only about 350 JFCs and 50 HFCs are known. LSST will discover on the order of 10,000 comets, with 50 observations or more of each of them (Solontoi et al. 2009). This will dwarf the current roster, providing answers to many questions regarding the physical properties of today's cometary population.

The size distribution will tell us about the competing evolutionary processes that affect a comet's radius, e.g., its creation as a collisional fragment, its self-erosion from activity, and its stochastic ejection of significant fragments. The shape of the JFC size distribution is starting to be understood (for example, Meech et al. 2004), although there are still strong discovery biases in the known population, as evinced by the fact that many large JFCs (3-4 km radius) with perihelia beyond 2 AU have only been discovered in the last few years (Fernández et al. 2008). LSST will provide us with a much more complete survey of the JFC population, since it will see 400-m radius inactive nuclei at 3 to 4 AU and even 1-km radius nuclei at 6 AU (the typical JFC aphelion). Perhaps even more important will be LSST's discoveries of HFCs and LPCs. The size distributions of these groups are completely unknown, suffering from low-number statistics and the fact that these comets are discovered or recovered inbound only after they have become active.

While adequately explaining the measured color distributions of TNOs and Centaurs has proved challenging, the dichotomy between TNO/Centaur colors and cometary colors is striking (Jewitt 2002; Grundy 2009). Cometary nuclei seem to be on average less red than their outer Solar System counterparts. In the case of the JFCs, the nuclei are presumably direct descendants of Centaurs and TNOs, so understanding how a comet's surface changes as it migrates deeper into the center of the Solar System is an important question. Perhaps cometary activity rapidly changes surface properties, but if so, then there should be a correlation between colors of comets and active

Centaurs. In addition to finding TNOs and Centaurs that are closer in size to cometary nuclei, LSST will provide us with a large number of cometary colors with which to make statistically strong comparisons. In particular, LSST will let us measure the colors of HFCs and LPCs, a field that is right now almost totally unexplored. A very exciting possibility is that LSST will discover some "new-in-the-Oort-sense" LPCs that have not yet turned on, giving us an opportunity to study a cometary surface unchanged from its time in the deep freeze of the Oort Cloud.

Traditionally, comets were thought to "turn off" beyond 3 AU, but in recent years that paradigm has started to change as we observe low but definitely non-zero mass loss from comets even all the way to aphelion in the case of JFCs (e.g., Snodgrass et al. 2008; Mazzotta Epifani et al. 2008) and out beyond 25 AU in the case of Hale-Bopp (Szabó et al. 2008). LSST's 10-year lifespan and deep magnitude limit will allow us to monitor many comets for outgassing activity over a significant interval of time (and for JFCs, over all or nearly all their orbits). The excellent spatial resolution will let us monitor even low levels of activity using point spread function comparisons, where the comet shows some coma that extends just slightly beyond the seeing disk. LSST will also be able to address how long comets stay active after perihelion and for what fraction of comets is crystallization of water ice and/or supervolatile sublimation a source of energy at high heliocentric distances.

Understanding the gas-to-dust ratio of comets and how this varies among comets of different dynamical classes and ages could let us understand the nature of the cometary activity process itself. The LSST u-band peaks near the CN violet (0-0) band at 387 nm. While CN is not the most abundant dissociation product from cometary volatiles, its violet band is second in intrinsic brightness only to the OH (0-0) band at 309 nm, which is much harder to observe. Thus CN emission can be used as a proxy for the overall gas production rate. This u-band throughput peak occurs at the longward edge of the bandpass; the rest of the bandpass will detect shorter wavelength continuum, and since a comet's continuum is reflected sunlight, it gets weaker toward the violet and near-UV. So the u-band will be particularly sensitive to a comet's gas coma. In combination with the r, i, z, and y bandpasses, which will be mostly sensitive to the continuum, a comet's colors should yield a rough estimate of the CN band strength and hence an approximate CN production rate. Thus LSST provides the very exciting opportunity to produce a large database of CN production rates for the known comets and for many of the new comets that it will discover. Existing databases (A'Hearn et al. 1995; Schleicher & Bair 2008) will not be able to match the size of an LSST-produced catalog. Trends of the gas-to-dust ratio as a function of other parameters – perihelion distance, heliocentric distance, active fraction, statistical age, dynamical group – will give clues about how pulsed insolation affects the evolution of a comet's surface.

5.10 Mapping of Interplanetary Coronal Mass Ejections

Bojan Vršnak, Željko Ivezić

Large-scale solar eruptions, called coronal mass ejections (CMEs), are the most powerful explosive events in the Solar System, where the total released energy can be as high as 10^{26} J. During the eruption, a magnetic flux of the order 10^{23} Weber is launched into interplanetary space at velocities of the order of 1000 km s^{-1}, carrying along $10^{11} - 10^{14}$ kg of coronal plasma. The Earth-directed CMEs, and the shocks they drive, are the main source of major geomagnetic storms (Gosling et al.

1990), so understanding their propagation through interplanetary space is one of central issues of Space Weather research.

The propagation of CMEs in the high corona can be traced by space-borne coronagraphs onboard spacecraft missions such as the Solar and Heliospheric Observatory (SoHO) and the Solar Terrestrial Relations Observatory (STEREO). At larger heliocentric distances, the interplanetary counterparts of CMEs (hereafter ICMEs) can be followed with very high sensitivity coronagraphs onboard STEREO and Solar Mass Ejection Imager (SMEI) missions, by mapping the interplanetary scintillation of distant radio sources (Manoharan 2006), or by employing the long-wavelength radio type II bursts excited at shocks that are driven by ICMEs (Reiner et al. 2007). The physical characteristics of ICMEs can also be directly determined by in situ measurements of various space probes that register solar wind characteristics.

LSST will offer a novel method for three dimensional mapping of ICME propagation, when combined with in situ solar wind measurements. This method has already been applied, although in a very limited form, in the 1970s (Dryer et al. 1975). The cometary plasma is affected by the passage of an ICME due to the enhanced ram and magnetic-field pressure associated with the ICME. This causes sudden changes of the cometary brightness and morphological changes of the coma and the tail[2] (Dryer et al. 1975, 1976). The comprehensive spatial and temporal LSST sky coverage will locate a sufficient number of comets that could be used as probes to detect passages of ICMEs. The three-day time resolution of the LSST deep-wide-fast survey is sufficient to track ICME-forced changes at distances larger than a few AU (Dryer et al. 1975). At closer distances the changes could be monitored by a network of large amateur telescopes, which will be provided by the comet positions from LSST, as well as by monitoring comet activity by STEREO and SMEI.

The unprecedented capabilities of LSST, in combination with comet observations by STEREO and SMEI, as well as by follow-up observations by networks of telescopes such as those anticipated for the Las Cumbres Observatory, will provide a high-quality monitoring of a large number of comets, and enable exquisite three dimensional mapping of the ICME activity in interplanetary space. The detected passages of ICMEs and their shocks will be used to:

- measure kinematic properties of the ICME propagation (position and velocity as functions of time), which will provide valuable information about forces acting on ICMEs;
- determine the angular extent of ICMEs and their shocks;
- estimate the distance range up to which ICMEs preserve their identity; and
- study interaction of cometary plasma with solar wind.

5.11 The NEA Impact Hazard

Alan W. Harris, R. Lynne Jones

Although the possibility of a catastrophic impact of an asteroid or comet with the Earth has been recognized for decades and even centuries (Edmund Halley articulated the possibility in his publication of the orbit of the comet that now bears his name), only in the past few decades have

[2]For an impressive demonstration, please see http://smei.nso.edu/images/CometHolmes.mpg.

surveys targeted Near Earth Asteroids (NEAs) with the specific intent of cataloging all or as many objects as possible in order to understand this risk.

In 2005, Congress issued a mandate calling for the detection and tracking of 90% of all NEAs larger than 140 m in diameter by 2020. This has typically been interpreted as applying to 90% of all Potentially Hazardous Asteroids (PHAs), which are NEAs with a perihelion distance of less than 1.3 AU. The date deadline was chosen to be 15 years after signing the mandate, which at the time seemed a reasonable period to build a system (either space or Earth-based) to catalog these PHAs. The size limit (140 m in diameter) and completeness level (90%) were chosen through a careful calculation of potential risks from impactors, weighed against increasing costs to detect smaller and smaller objects, as well as a consideration for previous cataloging efforts.

Previous and on-going surveys such as Spacewatch and the Catalina Sky Survey have already come close to identifying 90% of all PHAs larger than 1 km in diameter (NASA's so-called "Spaceguard" goal), using modest sized (< 2m) telescopes with limiting magnitudes in the range of $V \sim 21$. These 1 km PHAs would be capable of causing global catastrophe if one impacted the Earth. To date, over 800 PHAs have been detected above this size limit and while tracking must be ongoing (particularly for objects which pass particularly close to gravitational perturbation sources such as Earth), none is currently known to be on an impacting orbit.

However, smaller PHAs certainly could be on impact trajectories. This was recently brought home by the asteroid 2008 TC_3, detected less than 24 hours before it entered the Earth's atmosphere, ultimately impacting in a remote part of Sudan (Jenniskens et al. 2009; McGaha et al. 2008; Chesley et al. 2008). While 2008 TC_3 was a small PHA and impacts of this size are actually fairly common, it does illustrate that the possibility exists for larger PHAs to hit the Earth. By cataloging all PHAs above 140 m in diameter, the congressional mandate is intended to increase our awareness of potential risk in terms of death and property damage by approximately an order of magnitude beyond that which had been posed by 1 km objects. Figure 5.10 and its caption describes more of the hazards posed by various sizes of PHAs.

Technology has improved beyond that available when the 2005 Congressional mandate was issued, although the funding available to fulfill this mandate has not materialized. A 140 m PHA has an absolute magnitude of approximately $H = 22$. Integrating models of the orbital distribution of PHAs to determine their positions and distances indicate that 10% of PHAs larger than 140 m never become brighter than $V = 23.5$ over a 10 year period. In addition, PHAs can move up to a few degrees per day, thus requiring detection during short exposure times. This short exposure time, coupled with this required limiting magnitude and the necessary sky coverage, requires a system with a large field of view and sensitive detection limit. LSST has the potential to reach the goal of detecting 90% of all PHAs larger than 140 m by 2028, as described in § 5.11.1.

5.11.1 The NEA Completeness Analysis

Željko Ivezić

To assess the LSST completeness for PHAs, the PHA population is represented by a size-limited complete sample of 800 true PHAs whose orbital elements are taken from the Minor Planet Center. The simulated baseline survey is used to determine which PHAs are present in each exposure and

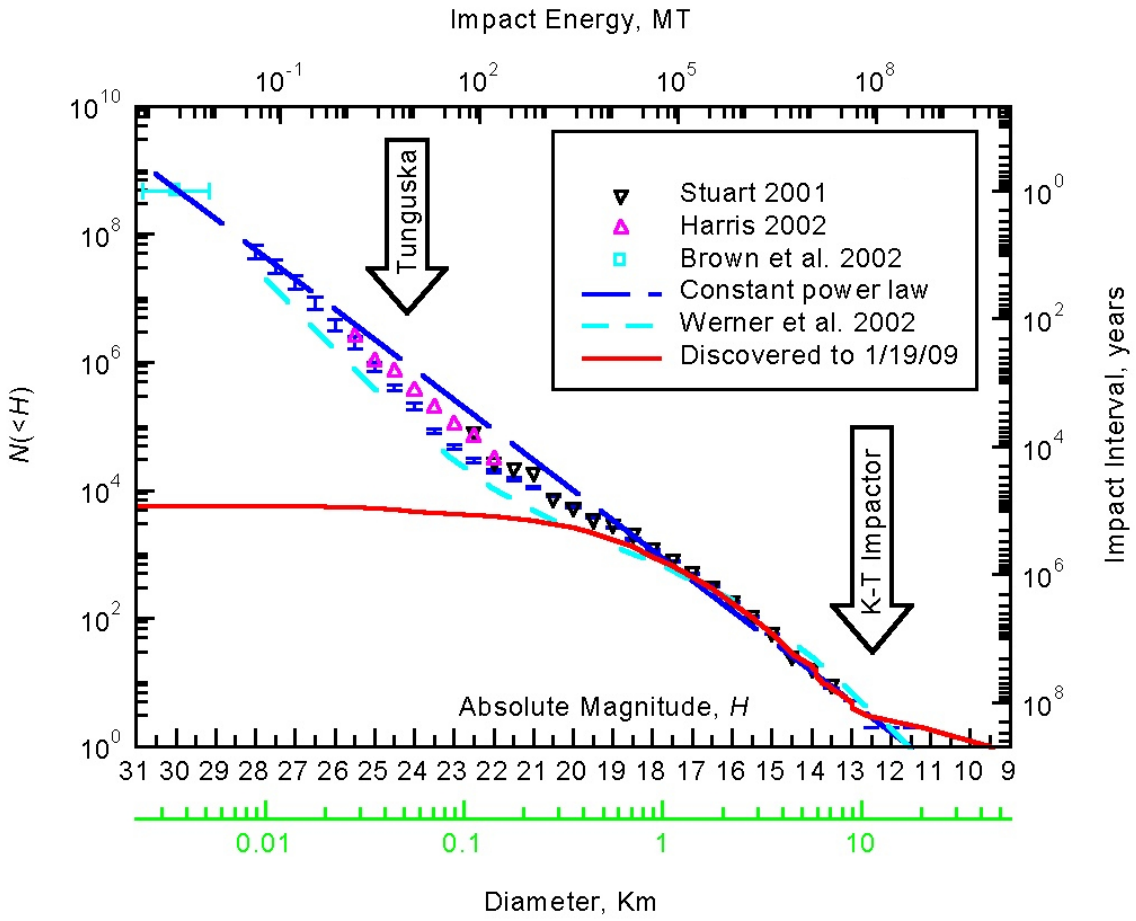

Figure 5.10: Various estimates of the size vs. impact frequency of NEAs (dashed lines). Equivalent astronomical absolute magnitude and impact in megatons are shown. The potential damage from a cosmic impact can be divided roughly into four categories. Below a diameter of ~ 30 m, incoming bodies explode high enough in the atmosphere that no ground damage occurs in the form of a blast wave. In the next size range extending up to 100-150 m or so, most of the impact energy is released in the atmosphere resulting in ground damage more or less similar to a large nuclear blast. Over land this has the potential to create major devastation as can be seen by the scar of the Tunguska event of a century ago. Even larger events in which the incoming body would reach the ground still traveling at cosmic velocity would cause even greater damage over land, but it is expected that the larger risk in this size range is from tsunami from impacts occurring into the ocean. At some size, variously estimated between 1 and 2 km diameter, it is expected that the impact event would lead to a global climatic catastrophe (for either land or sea impact) due to dust lofted into the stratosphere, with the possibility of ending civilization, perhaps killing a quarter or more of the human population from famine, disease, and general failure of social order. An example of this mass-extinction level event is the K-T Impactor. (Alan W. Harris, modified from http://neo.jpl.nasa.gov/neo/report2007.html).

at what signal-to-noise ratio they were observed. In addition to seeing, atmospheric transparency, and sky background effects, the signal-to-noise computation takes into account losses due to non-optimal filters and object trailing. Using SDSS observations of asteroids (Ivezić et al. 2001), we adopt the following mean colors to transform limiting (AB) magnitudes in LSST bandpasses to an 'effective' limiting magnitude in the standard V band: $V - m = (-2.1, -0.5, 0.2, 0.4, 0.6, 0.6)$ for $m = (u, g, r, i, z, y)$. Due to very red $V - u$ colors, and the relatively bright limiting magnitude in the y band, the smallest objects are preferentially detected in the $griz$ bands. The correction for

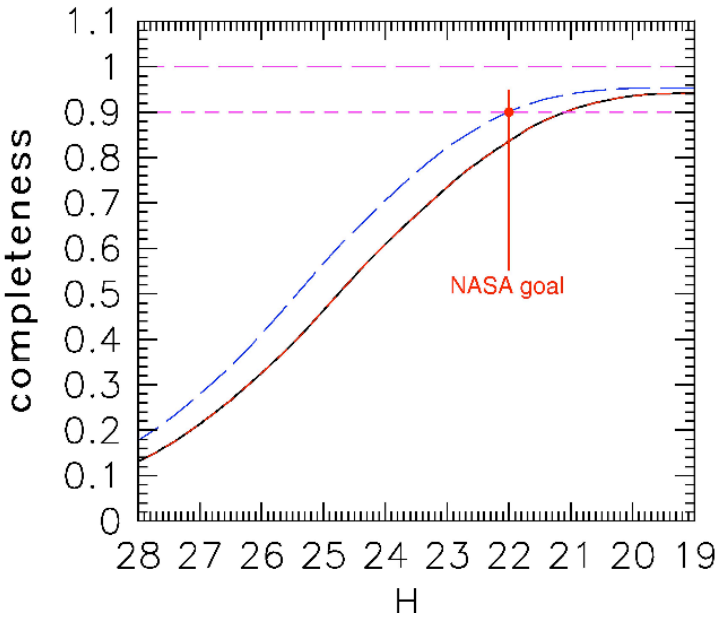

Figure 5.11: Completeness of the LSST survey for PHAs brighter than a given absolute magnitude (related to the size of the object and albedo; H=22 mag is equivalent to a typical 140 m asteroid and H=24 mag is equivalent to a 50 m asteroid). Two scenarios are shown: the lower curve is the 10-year long baseline survey where 5% of the total observing time is spent on NEA-optimized observations in the Northern Ecliptic (NE) region, and it reaches a completeness of 84% after 10 years. The upper dashed curve results from spending 15% of the observing time in an NEA-optimized mode, and running the survey for 12 years. It meets the 90% completeness level for 140 m objects mandated by the U.S. Congress.

trailing is implemented by subtracting from the $5\,\sigma$ limiting magnitude for point sources

$$\Delta m_5^{\rm trailing} = 1.25\,\log_{10}\left(1 + 0.0267\frac{v\,t_{vis}}{\theta}\right), \tag{5.5}$$

where the object's velocity, v, is expressed in deg/day. For the nominal exposure time (t_{vis}) of 30 seconds and seeing $\theta = 0.7''$, the loss of limiting magnitude is 0.16 mag for $v = 0.25$ deg day^{-1}, typical for objects in the main asteroid belt, and 0.50 mag for $v = 1.0$ deg day^{-1}, typical of NEAs passing near Earth.

The completeness of LSST in cataloging NEAs was calculated by propagating a model NEA source population (taken from the MOPS Solar System model, as in § 2.5.3), over the lifetime of the LSST survey mission, and simply counting the number of times LSST would be expected to detect the object under a variety of methods of operation (more on these observing cadences below). An object's orbit is considered to be cataloged if the object was detected on at least three nights during a single lunation, with a minimum of two visits per night. The same criterion was used in NASA studies[3], and is confirmed as reliable by a detailed analysis of orbital linking and determination using the MOPS code (§ 2.5.3). The MOPS software system and its algorithms are significantly more advanced than anything fielded for this purpose to date. Realistic MOPS simulations show $> 99\%$ linking efficiency across all classes of Solar System objects.

[3]The NASA 2007 NEA study is available from http://neo.jpl.nasa.gov/neo/report2007.html.

For the LSST baseline cadence (§ 2.1), objects counted as cataloged are observed on 20 different nights on average over ten years. A more stringent requirement that an object must be detected on at least five nights decreases the completeness by typically 3%. The completeness is also a function of the assumed size distribution of NEAs: the flatter the distribution, the higher the completeness. If the latest results for the NEA size distribution by Alan W. Harris (personal communication) are taken into account, the completeness increases by 1-2%. Due to these issues, the completeness estimates have a systematic uncertainty of at least 2%. Once the completeness rises above 60%, an increase in 10% in completeness corresponds to roughly a decrease of one magnitude in H.

The LSST baseline cadence provides orbits for 82% of PHAs larger than 140 m after 10 years of operations. With a minor change of this cadence, such as requiring that all observations in the so-called North Ecliptic (NE) region, defined by $\delta > 5°$) are obtained in the r band, the completeness for 140 m and larger PHAs is 84%, with 90% completeness reached for 200 m and larger objects. The completeness curve as a function of an object's size is shown in Figure 5.11 (lower curve). The observing cadence described here spends only 5% of the total observing time on NEA-optimized observations in the NE region.

Various adjustments to the baseline cadence can boost the completeness for 140 m and larger PHAs to 90%. We find that such variations can have an unacceptably large impact on other science programs, if the 90% completeness is to be reached within the 10 year survey lifetime. However, with a minor adjustment of the baseline cadence, such that 15% of the time is spent in the NE region to reach fainter limiting magnitudes, this completeness level can be reached with a 12-year long survey, and with a negligible effect on other science goals. The completeness curve as a function of an object's size for such a modified cadence is shown in Figure 5.11 (upper curve).

Our analysis assumes that no NEAs are known prior to LSST. Currently known NEAs do not have a significant impact on this calculation. However, if a precursor survey, such as Pan-STARRS 4, operated for three years prior to LSST, the time to fulfill the Congressional mandate by LSST could be shortened by about a year.

5.12 NEAs as Possible Spacecraft Mission Targets

Paul A. Abell

LSST has the capability of detecting and characterizing more than 90% of the NEAs equal to, or larger than 140 m in diameter in just 12 years of operation. This is not only important for characterizing the potential impact threat from these objects, but these observations will also provide a wealth of information on possible spacecraft targets for future investigation. NEAs are objects of interest from a hazard perspective given that their orbits can bring them into close proximity with the Earth. However, this makes them prime candidates for in situ investigation given that they are also some of the easiest objects to reach in the Solar System. These objects have relatively low velocities relative to Earth (5 to 7 km s^{-1}) and are good targets for possible future science and sample return missions. NASA's NEAR Shoemaker spacecraft to (433) Eros, JAXA's Hayabusa probe to (25143) Itokawa, and ESA's Rosetta mission to comet 67P/Churyumov-Gerasimenko are examples of the types of missions that can be sent to NEAs. Given that a subset of the total NEA population has orbital parameters similar to that of the Earth (i.e., low inclination

and low eccentricity), new discoveries made by LSST will expand the currently known target list for future robotic and human-led spacecraft missions.

NASA's Constellation Program is developing the next generation of vehicles for human exploration, as mandated by the United States Space Exploration Policy. These vehicles are currently under development for missions to the International Space Station (ISS) and the Moon. However, these missions are not the only ones currently under consideration at NASA. Crewed voyages to NEAs are also being analyzed as possible alternative missions for NASA. The 2009 Augustine Committee review of U.S. human spaceflight plans has included NEAs as high-profile astronaut destinations in several of its exploration options. In addition, an agency-sponsored internal study has determined that the new Constellation vehicles have the capability to reach several NEAs, conduct detailed scientific and exploration operations of these objects, and return to Earth after 180 days. Using the existing NEA database, currently only about ten known targets are reachable using NASA's Constellation systems within the desired 2020 to 2035 time-frame. New data from LSST would expand this list of dynamically viable targets by more than an order of magnitude and help to refine target selection based on the observed physical characteristics (taxonomy, rotation state, etc.) of the objects discovered. LSST is uniquely qualified for this type of effort given its sensitivity for detecting and characterizing NEAs.

The next stages in the human exploration and exploitation of space will be highly dependent on the feasibility of extracting materials (primarily water and minerals) from in situ sources. In addition, to their accessibility from Earth, NEAs are potentially the most cost-efficient sources for providing propulsion and life support, and for building structures in space. It is highly probable that the success and viability of human expansion into space beyond low-Earth orbit depends on the ability to exploit these potential resources. Therefore, a detailed physical and compositional assessment of the NEA population will be required before any human missions are sent to these objects. LSST will be a key asset in NEA discovery and play a significant role in the initial reconnaissance of potential NEA resources necessary for future human exploration of the Solar System.

References

Abell, P. A. et al., 2005, *Icarus*, 179, 174

A'Hearn, M. F., Millis, R. L., Schleicher, D. G., Osip, D. J., & Birch, P. V., 1995, *Icarus*, 118, 223

Allen, R. L., Gladman, B., Kavelaars, J. J., Petit, J.-M., Parker, J. W., & Nicholson, P., 2006, *ApJL*, 640, L83

Asher, D. J., Bailey, M. E., Hahn, G., & Steel, D. I., 1994, *MNRAS*, 267, 26

Bailey, M. E., & Emel'Yanenko, V. V., 1996, *MNRAS*, 278, 1087

Bernstein, G. M., Trilling, D. E., Allen, R. L., Brown, M. E., Holman, M., & Malhotra, R., 2004, *AJ*, 128, 1364

Binzel, R. P., 1994, in Astronomical Society of the Pacific Conference Series, Vol. 63, 75 Years of Hirayama Asteroid Families: The Role of Collisions in the Solar System History, Y. Kozai, R. P. Binzel, & T. Hirayama, eds., p. 251

Bottke, W. F., Morbidelli, A., Jedicke, R., Petit, J.-M., Levison, H. F., Michel, P., & Metcalfe, T. S., 2002, *Icarus*, 156, 399

Bottke, Jr., W. F., Vokrouhlický, D., Rubincam, D. P., & Nesvorný, D., 2006, Annual Review of Earth and Planetary Sciences, 34, 157

Bowell, E., 2009, VizieR Online Data Catalog, 1, 2001

Brasser, R., Duncan, M. J., & Levison, H. F., 2008, *Icarus*, 196, 274

Brown, M. E., Barkume, K. M., Ragozzine, D., & Schaller, E. L., 2007, *Nature*, 446, 294

Brown, M. E., Trujillo, C., & Rabinowitz, D., 2004, *ApJ*, 617, 645

Brown, M. E. et al., 2006, *ApJL*, 639, L43

Chesley, S., Chodas, P., & Yeomans, D., 2008, Asteroid 2008 TC3 Strikes Earth: Predictions and Observations Agree. http://neo.jpl.nasa.gov/news/2008tc3.html
DeMeo, F., & Binzel, R. P., 2008, *Icarus*, 194, 436
Disanti, M. A., & Mumma, M. J., 2008, *Space Science Reviews*, 138, 127
Domingue, D., & Hapke, B., 1989, *Icarus*, 78, 330
Doressoundiram, A., Boehnhardt, H., Tegler, S. C., & Trujillo, C., 2008, Color Properties and Trends of the Transneptunian Objects, The Solar System Beyond Neptune, pp. 91–104
Doressoundiram, A., Peixinho, N., Doucet, C., Mousis, O., Barucci, M. A., Petit, J. M., & Veillet, C., 2005, *Icarus*, 174, 90
Dryer, M., Ershkovich, A. I., & Shen, W.-W., 1976, *Journal of Geophysical Research*, 81, 6184
Dryer, M., Eviatar, A., Frohlich, A., Jacobs, A., Joseph, J. H., & Weber, E. J., 1975, *Journal of Geophysical Research*, 80, 2001
Duncan, M. J., 2008, *Space Science Reviews*, 138, 109
Durda, D. D., & Dermott, S. F., 1997, *Icarus*, 130, 140
Durech, J., Grav, T., Jedicke, R., Denneau, L., & Kaasalainen, M., 2005, *Earth Moon and Planets*, 97, 179
Durech, J., & Kaasalainen, M., 2003, *A&A*, 404, 709
Durech, J., Scheirich, P., Kaasalainen, M., Grav, T., Jedicke, R., & Denneau, L., 2007, in IAU Symposium, Vol. 236, IAU Symposium, G. B. Valsecchi, D. Vokrouhlický, & A. Milani, eds., pp. 191–200
Elliot, J. L. et al., 2005, *AJ*, 129, 1117
Fernandez, J. A., 1997, *Icarus*, 129, 106
Fernández, Y. R., Jewitt, D. C., & Sheppard, S. S., 2005, *AJ*, 130, 308
Fernández, Y. R. et al., 2008, *LPI Contributions*, 1405, 8307
Funato, Y., Makino, J., Hut, P., Kokubo, E., & Kinoshita, D., 2004, *Nature*, 427, 518
Gladman, B., & Chan, C., 2006, *ApJL*, 643, L135
Gladman, B., Holman, M., Grav, T., Kavelaars, J., Nicholson, P., Aksnes, K., & Petit, J.-M., 2002, *Icarus*, 157, 269
Gladman, B. et al., 2009, *ApJL*, 697, L91
Gladman, B., Marsden, B. G., & Vanlaerhoven, C., 2008, Nomenclature in the Outer Solar System, The Solar System Beyond Neptune, pp. 43–57
Goldreich, P., Lithwick, Y., & Sari, R., 2002, *Nature*, 420, 643
Gomes, R., Levison, H. F., Tsiganis, K., & Morbidelli, A., 2005, *Nature*, 435, 466
Gomes, R. S., 2003, *Icarus*, 161, 404
Gomes, R. S., Morbidelli, A., & Levison, H. F., 2004, *Icarus*, 170, 492
Gosling, J. T., Bame, S. J., McComas, D. J., & Phillips, J. L., 1990, *Geophysical Research Letters*, 17, 901
Gradie, J. C., Chapman, C. R., & Tedesco, E. F., 1989, in Asteroids II, R. P. Binzel, T. Gehrels, & M. S. Matthews, eds., pp. 316–335
Gradie, J. C., Chapman, C. R., & Williams, J. G., 1979, Families of minor planets, T. Gehrels, ed., pp. 359–390
Grav, T., Holman, M. J., Gladman, B. J., & Aksnes, K., 2003, *Icarus*, 166, 33
Grav, T., Jedicke, R., Denneau, L., Holman, M., Spar, T. B., & Chesley, S., 2009, in preparation
Grundy, W. M., 2009, *Icarus*, 199, 560
Hahn, J. M., & Malhotra, R., 2005, *AJ*, 130, 2392
Harris, A. W., & Pravec, P., 2006, in IAU Symposium, Vol. 229, Asteroids, Comets, Meteors, L. Daniela, M. Sylvio Ferraz, & F. J. Angel, eds., pp. 439–447
Hirayama, K., 1918, *AJ*, 31, 185
Hsieh, H. H., & Jewitt, D., 2006, *Science*, 312, 561
Ida, S., Larwood, J., & Burkert, A., 2000, *ApJ*, 528, 351
Ivezić, Ž. et al., 2008, ArXiv e-prints, 0805.2366
Ivezić, Ž. et al., 2002, *AJ*, 124, 2943
—, 2001, *AJ*, 122, 2749
Jedicke, R., & Metcalfe, T. S., 1998, *Icarus*, 131, 245
Jenniskens, P. et al., 2009, *Nature*, 458, 485
Jewitt, D., 1996, *Earth Moon and Planets*, 72, 185
—, 2005, *AJ*, 129, 530
Jewitt, D. C., 2002, *AJ*, 123, 1039
Jones, R. L., Parker, J. M., Bieryla, A., Marsden, B. G., Gladman, B., Kavelaars, J., & Petit, J. M., 2009, *AJ*, submitted
Jurić, M. et al., 2002, *AJ*, 124, 1776

Kaasalainen, M., 2004, *A&A*, 422, L39
Kaasalainen, M., & Torppa, J., 2001, *Icarus*, 153, 24
Kaasalainen, M., Torppa, J., & Muinonen, K., 2001, *Icarus*, 153, 37
Kaib, N. A. et al., 2009, *ApJ*, 695, 268
Kaib, N. A., & Quinn, T., 2008, *Icarus*, 197, 221
—, 2009, *Science*, 325, 1234
Kavelaars, J., Jones, L., Gladman, B., Parker, J. W., & Petit, J.-M., 2008, The Orbital and Spatial Distribution of the Kuiper Belt, The Solar System Beyond Neptune, pp. 59–69
Kenyon, S. J., & Bromley, B. C., 2004, *Nature*, 432, 598
Kryszczyńska, A., La Spina, A., Paolicchi, P., Harris, A. W., Breiter, S., & Pravec, P., 2007, *Icarus*, 192, 223
Lacerda, P., & Jewitt, D. C., 2007, *AJ*, 133, 1393
Lada, C. J., & Lada, E. A., 2003, *ARAA*, 41, 57
Levison, H. F., Bottke, W., Gounelle, M., Morbidelli, A., Nesvorny, D., & Tsiganis, K., 2008a, AAS/Division of Dynamical Astronomy Meeting, Vol. 39, Chaotic Capture of Planetesimals into Regular Regions of the Solar System. II: Embedding Comets in the Asteroid Belt. p. 12.05
Levison, H. F., Duncan, M. J., Dones, L., & Gladman, B. J., 2006, *Icarus*, 184, 619
Levison, H. F., Morbidelli, A., Vanlaerhoven, C., Gomes, R., & Tsiganis, K., 2008b, *Icarus*, 196, 258
Levison, H. F., Morbidelli, A., Vokrouhlický, D., & Bottke, W. F., 2008c, *AJ*, 136, 1079
Lunine, J. I., 1993, *Science*, 261, 697
Malhotra, R., 1995, *AJ*, 110, 420
Manoharan, P. K., 2006, *Solar Physics*, 235, 345
Marchis, F., Kaasalainen, M., Hom, E. F. Y., Berthier, J., Enriquez, J., Hestroffer, D., Le Mignant, D., & de Pater, I., 2006, *Icarus*, 185, 39
Mazzotta Epifani, E., Palumbo, P., Capria, M. T., Cremonese, G., Fulle, M., & Colangeli, L., 2008, *MNRAS*, 390, 265
McFadden, L. A., Gaffey, M. J., & McCord, T. B., 1985, *Science*, 229, 160
McGaha, J. E. et al., 2008, Minor Planet Electronic Circulars, 50
Meech, K. J., Hainaut, O. R., & Marsden, B. G., 2004, *Icarus*, 170, 463
Minton, D. A., & Malhotra, R., 2009, *Nature*, 457, 1109
Morbidelli, A., & Gladman, B., 1998, *Meteoritics and Planetary Science*, 33, 999
Morbidelli, A., & Levison, H. F., 2004, *AJ*, 128, 2564
Morbidelli, A., Levison, H. F., Tsiganis, K., & Gomes, R., 2005, *Nature*, 435, 462
Nagasawa, M., Tanaka, H., & Ida, S., 2000, *AJ*, 119, 1480
Noll, K. S., Grundy, W. M., Chiang, E. I., Margot, J.-L., & Kern, S. D., 2008, Binaries in the Kuiper Belt, The Solar System Beyond Neptune, pp. 345–363
O'Brien, D. P., & Greenberg, R., 2005, *Icarus*, 178, 179
O'Brien, D. P., Morbidelli, A., & Bottke, W. F., 2007, *Icarus*, 191, 434
Parker, A., Ivezić, Ž., Jurić, M., Lupton, R., Sekora, M. D., & Kowalski, A., 2008, *Icarus*, 198, 138
Peale, S. J., 1993, *Icarus*, 106, 308
Petit, J.-M., Morbidelli, A., & Chambers, J., 2001, *Icarus*, 153, 338
Petit, J.-M., Morbidelli, A., & Valsecchi, G. B., 1999, *Icarus*, 141, 367
Reiner, M. J., Kaiser, M. L., & Bougeret, J.-L., 2007, *ApJ*, 663, 1369
Schleicher, D. G., & Bair, A. N., 2008, LPI Contributions, 1405, 8174
Sheppard, S. S., & Jewitt, D., 2004, *AJ*, 127, 3023
Sheppard, S. S., Lacerda, P., & Ortiz, J. L., 2008, Photometric Lightcurves of Transneptunian Objects and Centaurs: Rotations, Shapes, and Densities, The Solar System Beyond Neptune, pp. 129–142
Snodgrass, C., Lowry, S. C., & Fitzsimmons, A., 2008, *MNRAS*, 385, 737
Solontoi, M. et al., 2009, *Icarus*, 10.1016/j.icarus.2007.11.033
Stern, S. A., & Colwell, J. E., 1997, *AJ*, 114, 841
Szabó, G. M., Ivezić, Ž., Jurić, M., & Lupton, R., 2007, *MNRAS*, 377, 1393
Szabó, G. M., & Kiss, L. L., 2008, *Icarus*, 196, 135
Szabó, G. M., Kiss, L. L., & Sárneczky, K., 2008, *ApJL*, 677, L121
Taylor, R. C., & Tedesco, E. F., 1983, *Icarus*, 54, 13
Trujillo, C. A., Jewitt, D. C., & Luu, J. X., 2000, *ApJL*, 529, L103
—, 2001, *AJ*, 122, 457
Tsiganis, K., Gomes, R., Morbidelli, A., & Levison, H. F., 2005, *Nature*, 435, 459

Valsecchi, G. B., Carusi, A., Knezevic, Z., Kresak, L., & Williams, J. G., 1989, in Asteroids II, R. P. Binzel, T. Gehrels, & M. S. Matthews, eds., pp. 368–385
Vokrouhlický, D., Nesvorný, D., & Bottke, W. F., 2003, *Nature*, 425, 147
Weidenschilling, S. J., 2002, *Icarus*, 160, 212
Weissman, P. R., Bottke, Jr., W. F., & Levison, H. F., 2002, Evolution of Comets into Asteroids. pp. 669–686
Zappala, V., Bendjoya, P., Cellino, A., Farinella, P., & Froeschle, C., 1995, *Icarus*, 116, 291